**UNIVERSITY OF SOUTHAMPTON**

FACULTY OF NATURAL AND ENVIRONMENTAL SCIENCES

National Oceanography Centre, Southampton

School of Ocean and Earth Sciences

# Mixing in the Arctic Ocean:

Using the Advection-Diffusion Equation to estimate the role of diapycnal mixing in Arctic Ocean dynamics.

by

Romina DeGiorgio

Thesis for the degree of Master in Philosophy (MPhil.)

**December 2015**

**UNIVERSITY OF SOUTHAMPTON**

ABSTRACT

FACULTY OF NATURAL AND ENVIRONMENTAL SCIENCES
SCHOOL OF OCEAN AND EARTH SCIENCES

MASTER OF PHILOSOPHY

# MIXING IN THE ARCTIC OCEAN

by ROMINA DEGIORGIO

An advection – diffusion balance was used to calculate the diapycnal vertical mixing between water masses required to maintain the density stratification in the Arctic Ocean. A box model bounded by a velocity field created from hydrographic measurements at the gateways of the Arctic (Bering, Davis and Fram Strait and the Barents Sea Opening) was used, and the properties in the interior of the Arctic estimated from a climatology dataset (PHC). The density gradient, volume flux, vertical velocity, diapycnal diffusivity, and dissipation rate were calculated. A weak vertical velocity of $10^{-7}$ $ms^{-1}$ and a weak diapycnal mixing of ~2 x $10^{-6}$ $m^2$ $s^{-1}$ were found in the upper layers of the Arctic up to 200 m depth, likely due to weak turbulent mixing resulting from double diffusion, and consistent with microstructure measurements. An apparent negative diffusivity was found in the bottom layers. This is likely due to the effects of the warm, salty Atlantic Water inflow, of which 3.37 Sv enters the Arctic and is diapycnally transported into its adjacent layers, causing buoyancy loss from down-slope convection and densification of water.

# Table of Contents

# List of Figures

# List of Tables

# Declaration of Authorship

I, Romina DeGiorgio

declare that the thesis entitled

Mixing in the Arctic Ocean

and the work presented in the thesis are both my own, and have been generated by me as the result of my own original research. I confirm that:

- this work was done wholly or mainly while in candidature for a research degree at this University;
- where any part of this thesis has previously been submitted for a degree or any other qualification at this University or any other institution, this has been clearly stated;
- where I have consulted the published work of others, this is always clearly attributed;
- where I have quoted from the work of others, the source is always given. With the exception of such quotations, this thesis is entirely my own work;
- I have acknowledged all main sources of help;
- where the thesis is based on work done by myself jointly with others, I have made clear exactly what was done by others and what I have contributed myself;
- none of this work has been published before submission,

Signed:……..

Date:…….

# Graduate School of the
# National Oceanography Centre, Southampton

This MPhil. dissertation by

*Romina DeGiorgio*

Has been produced under the supervision of the following persons:

Supervisors:

- Prof. Alberto Naveira-Garabato
- Dr. Sheldon Bacon
- Dr. Jan Zika

Advisory Panel:

- Dr. Eleanor Frajka-Williams (Chair)

I would also to acknowledge Dr Takamasa Tsubouchi for his help especially in the initial stages of this project and for allowing me to use his calculated volume flux data, published in Tsubouchi *et al.* (2012). Prof. Tom Rippeth and Dr. Ben Lincoln provided the Microstructure data, published in Rippeth *et al.* (2015), and other useful information, for which I am very grateful.

# 1. **Introduction**

## 1.1 Aims & Project Rationale

The aims of this project are to estimate the turbulent vertical mixing with depth and the energy required to sustain this mixing in the Arctic Ocean using hydrographic data. A secondary aim is to analyze its origin by comparing it with the sources available to power this dissipation (mainly tides and wind).

Turbulent mixing transfers heat downward into the deep ocean and balances the cooling caused by deep water formation. Mixing is related through the buoyancy and vorticity equations to horizontal circulation and the intensity of upwelling. Vertical mixing estimates are very important and are required for numerical circulation models, predicting dispersion and for understanding the global circulation.

Direct measurements of mixing are generally unable to be used to define basin-scale averages as measurements are too sparse for large spatial areas. There are two fundamental methods to calculate eddy diffusivities indirectly from climatology data: approximating them from turbulence properties or by fitting an advection-diffusion equation to observations. During this project, an advection-diffusion equation was used.

The structure of the report is as follows: The first section is a review on the Arctic Ocean and its circulation followed by a summary of some the results from the Tsubouchi *et al.* (2012) paper on which this work is based, and an analysis of previous work on Arctic volume and heat transport. A literature review on mixing and deep water formation in the Arctic Ocean follows. The Methodology section describes the equations and model used, as well as the limitations and includes a brief summary of the data. The results are presented in Section 3 and discussed in Section 4, where they are compared with recent

Microstructure Measurements in the Arctic by Rippeth *et al*. (2015). Finally, Section 5 is a brief summary and conclusion of this work, with a few suggestions of possible further work.

## 1.2 Literature Review

### 1.2.1 The Arctic Ocean

The Arctic Ocean is a semi-enclosed marginal sea that connects with the North Atlantic and Pacific Oceans through several shallow and/or narrow passages (Figure 1). It is composed mainly of two basins – the Eurasian and Amerasian Basins, separated by the Lomonosov Ridge, and surrounded by extensive shelf areas. It connects with the North Atlantic Ocean by the relatively deep and narrow Fram Strait (depth of ~ 2600 m) and the shallower Barents Sea (200 – 300 m), as well as a network of narrow straits in the Canadian Arctic Archipelago (CAA), which empty in the 360 km wide and 650 m deep Davis Strait. Communication between the Arctic and the Pacific Ocean is restricted by the shallow (~50 m) and narrow (~85 km) Bering Strait.

The largest oceanic heat input to the Arctic Ocean results from the Atlantic Water (AW) inflow from the North Atlantic Ocean through the eastern part of Fram Strait and the Barents Sea Opening (BSO). Its relatively high salinity, and thus density, leads it to enter the Arctic at intermediate depths, between 200 and 400 m, after which it circulates cyclonically and topographically driven around the basin (Rudels *et al*. 1999; Aksenov *et al.* 2011, Spielhagen *et al.* 2011). Its core is ~4 $^{o}$C warmer than the overlying cold fresh halocline and surface mixed water and this creates a strong stratification which limits the penetration of surface-generated turbulence and isolates the ice cover from the AW heat.

The Arctic Ocean exports fresh buoyant surface waters as freshened cold seawater and sea ice to the North Atlantic through Fram Strait and the CAA (Aagaard & Carmack 1989;

Kwok 2009). It also creates and exports dense salty waters, and this formation of northern deep water is thought to be an important driving force of the global thermohaline circulation (Broecker 1991; Aagaard & Carmack 1994).

**0**

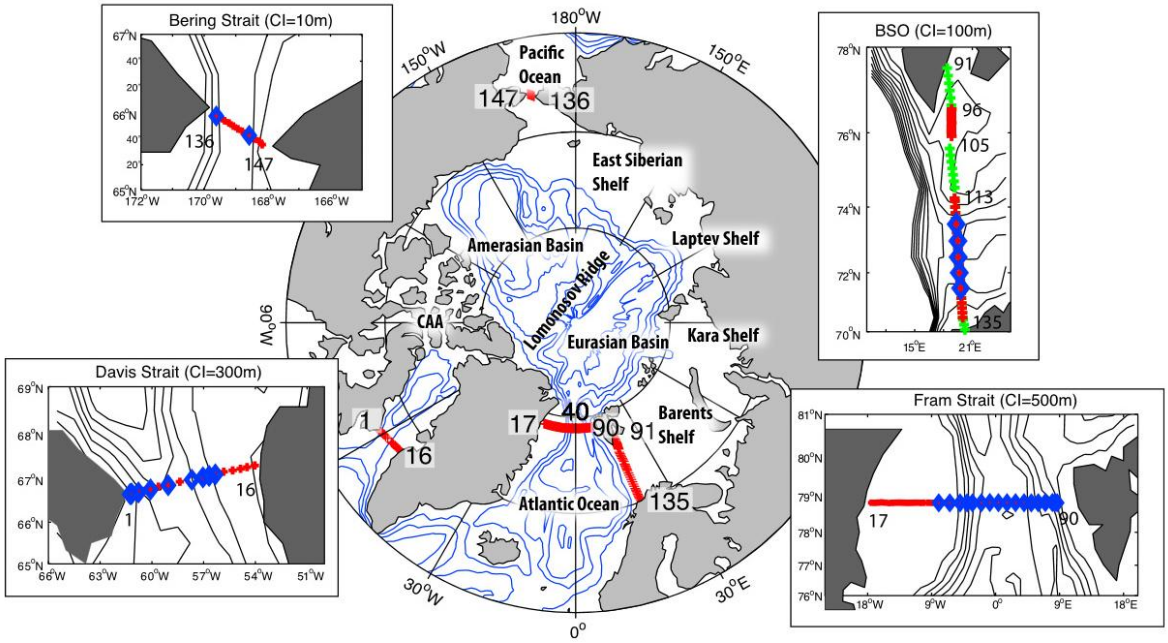


**Figure 1:** Bathymetric configuration in Davis, Fram and Bering Straits, and the Barents Sea Opening (BSO), showing CTD stations (red cross), model grid points (green cross), mooring locations (blue diamond) and station numbers (including model grid points). Major bathymetric features are shown (CAA – Canadian Arctic Archipelago). Bathymetric contour intervals (CI) for the Arctic figure is 1000 m, and the CI for each strait are shown (Tsubouchi *et al*. 2012).

The surface heat budget of the Arctic Ocean is driven by the local radiation balance and the surface reflectivity of ice. This and the storage and release of freshwater and greenhouse gases impact the global climate. The Arctic Ocean acts as a low salinity water reservoir and plays an important role in the global hydrological cycle. The Arctic Ocean receives a large fresh water input by river run-off from Siberia (especially by the rivers Lena, Ob and Yenesei) and North America (especially by the rivers Yukon and

Mackenzie). It also maintains its low salinity through precipitation, sea-ice melt and the inflow of relatively fresh water (FW) from the Pacific Ocean (Woodgate & Aagaard 2005). Various recent works have shown that the Arctic Ocean is changing, most likely in response to, and in association with, the changing climate. It is reported to be the fastest warming region of the planet (IPCC 2014) mainly due to the ice-albedo feedback leading to polar amplification (Manabe & Stouffer 1994; Serreze *et al.* 2009). Changes include, for example, warming of the Arctic atmosphere (Rigor *et al.* 2000) and an increase in the volume transport and warming of the AW in the Fram strait inflow (Carmack *et al.* 1995, 1997; Grotefendt *et al.* 1998; Morison *et al.* 1998; Schauer *et al.* 2002; Karcher *et al.* 2003; Polyakov *et al*. 2005). The mean Arctic sea surface temperature (SST) in September 2012 was 5 $^{o}$C higher than the 1997 – 2006 mean (Trofimov & Ingvaldsen 2013), leading to observations of substantial sea ice retreat (e.g. Steele *et al.* 2010, 2011; Jackson *et al*. 2012) and the record low of September sea-ice in 2012 (Jeffries *et al.* 2013).

Recent studies also show changes in the Arctic wide FW content (e.g. Polyakov *et al.* 2008), for example an increase in FW storage in the Arctic Ocean's upper layers (McPhee *et al.* 2009; Rabe *et al.* 2009) and a 25 % increase in Beaufort Gyre FW in 2013 compared to 1977 (Proshutinsky *et al.* 2009). This is possibly partly due to an increase in Russian river discharge into the Arctic (Shiklomanov & Lammers 2009) and an increase in the Pacific inflow. Climate simulations show that increased FW outflow from the Arctic may lead to reduced convection in the deep water formation regions of the North Atlantic, which may influence the Atlantic Meridional overturning circulation (Vellinga *et al.* 2008). The scarcity of observations in the Arctic, due to its remote location, extreme cold weather and ice cover conditions (which mean that the Arctic is inaccessible for much of the year), result in a poor knowledge of the Arctic circulation. Recent observations have shown that there is a much higher degree of spatial and temporal variability in the properties of the

Arctic Ocean than previously thought (Quadfasel *et al.* 1996; Carmack *et al.* 1997; Morison *et al.* 1998; Polyakov *et al.* 2004, 2005, 2008). Better understanding of the Arctic dynamics and circulation would improve knowledge of the consequences of possible changes to the Arctic due to warming of the global climate.

### 1.2.2 Summary of Conclusions from Tsubouchi *et al*. 2012

This study follows on from a paper published in 2012 by Tsubouchi *et al*. that assembled the available hydrographic observation and current measurements in the Arctic Ocean for summer 2005 A box inverse method was then applied to create a velocity field that conserves volume and salinity in order to estimate heat and FW transports and give a snapshot of the exchanges between the Arctic Ocean and the rest of the world oceans. A summary of the results is presented below, and details and a review of previous work can be found in the aforementioned paper.

#### *1.2.2.1 Water Mass Structure*

The Arctic Ocean is characterized by strong upper-ocean stratification, double diffusive layers and relatively deep waters (1000 – 2000 m), with well mixed homogenous bottom layers. It is salt stratified, which makes it vertically stable and allows the formation of sea ice and deep convection regions in the Labrador (Pickart *et al.* 2002), Greenland (Ronski & Budeus 2005), and Irminger Seas (Pickart *et al.* 2003).

Figure 2, taken from Tsubouchi *et al. (*2012), shows the distribution of potential temperature and salinity across the four main gateways of the Arctic. Fram Strait and the BSO show a similar distribution of south-going colder, fresher waters on the western side and warmer and saltier north-going waters on the east. The latter is caused by the inflow of AW. The temperature minimum in the subsurface layer at the west end of the two straits is recirculated and modified AW which has arrived there either via recirculating close to the

straits or via the long circuit around the Eurasian Basin. The deep water in Fram Strait (> 1000 m) has a small range of temperatures and salinities (~0.7 ± 0.1 $^{o}$C and 34.5 ± 0.01). The Davis Strait is occupied by relatively fresh waters, with warmer Atlantic Ocean-derived water in the eastern part. Surface meltwater runoff might cause the cooling of water on the western side . The Bering Strait is occupied by fresh and relatively warm Pacific Ocean-derived water.

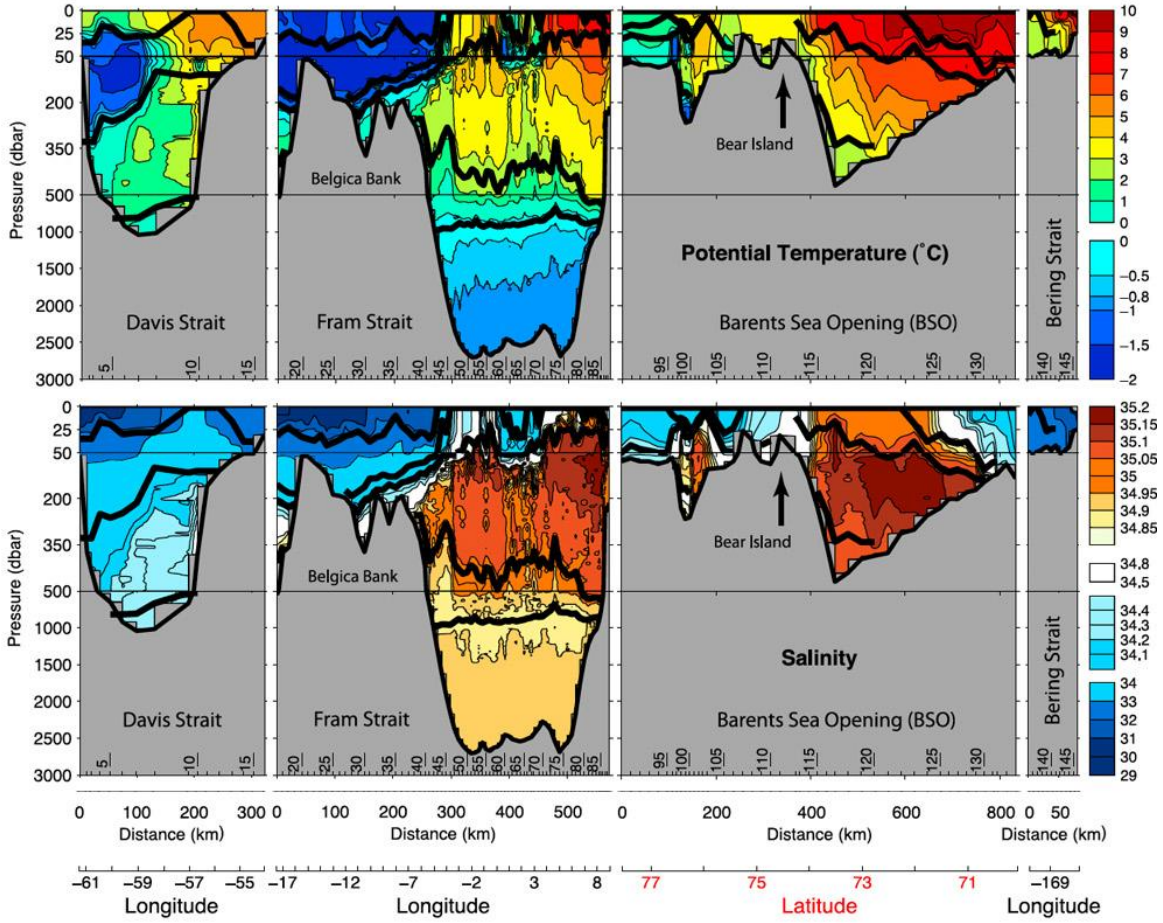


**Figure 2:** (top) Potential temperature and (bottom) salinity section along the Davis Strait, Fram Strait, the BSO and Bering Strait. Bold black lines show water mass boundaries and the color bar scale is nonlinear. The pressure axis is expanded between 0 and 50 dbar and 50 and 500 dbar and station numbers are shown along the base of each plot. (Plot from Tsubouchi *et al.* 2012).

### *1.2.2.2 Water Mass Transports and Heat and FW Fluxes in the Arctic Ocean*

The budget of seawater volume has been balanced by Tsubouchi *et al.* (2012) and the volume flux through the four gateways of the Arctic were calculated as: an inflow of +3.6 ± 1.1 Sv (1 Sv = $10^6$ $m^2s^{-1}$) through the BSO, a southward flow of -1.6 ± 3.9 Sv through Fram Strait, a volume flux of +1.0 ± 0.2 Sv in Bering Strait and an outflow of -3.1 ± 0.7 Sv through Davis Strait (Figure 3). Sign convention is negative for export (out of Arctic) and positive for import of water. The total Arctic heat flux was calculated as 189 ± 26 TW (Tsubouchi *et al.* 2012), with the main contribution (69 ± 13 TW) being through the AW layer.

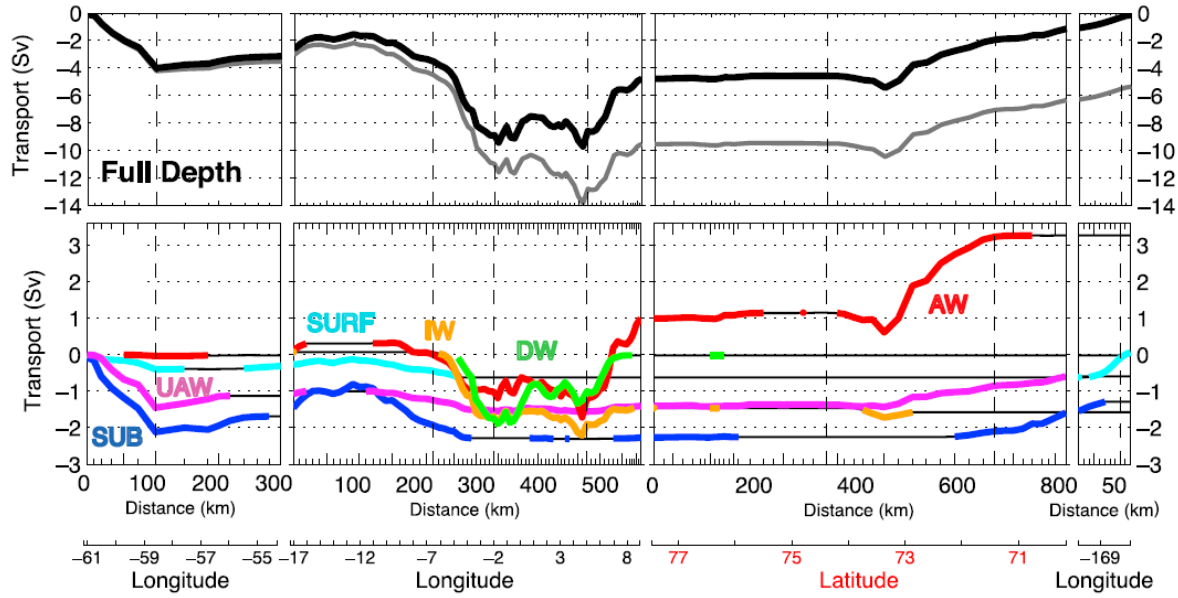


**Figure 3:** (top) Initial (gray) and final (black) full depth volume transport (Sv) accumulated around the boundary. (bottom) Accumulated volume transport for each water mass. Where a specific water mass is absent from the section, the accumulated transport is plotted as a black line. (Plot from Tsubouchi *et al.* 2012).

Table 1 shows a summary of the values of volume, heat and FW fluxes calculated by Tsubouchi *et al.* (2012), those calculated by Lique & Steele (2013) using a high-resolution global ocean sea-ice model to investigate Arctic Ocean heat content variability for the

period 1968 - 2007, and other work summarized in Lique & Steele (2013). These values show that the Arctic heat budget is highly variable on seasonal to inter-annual timescales, and that direct estimates made by different authors over different periods with different methods may vary widely.

**Table 1:** Summary of recent estimates of fluxes through the critical oceanic gateways, and their variability on different time scales. Values are positive for Arctic inflow. Bold values denote those taken from Tsubouchi *et al.* 2012, and used in this study

[1]The reference temperature is -0.23 [o]C, which is the mean temperature of the domain for this period. Means are calculated from monthly model output. Standard deviations are calculated from annual means. The sign convention is such that a source of heat into the Arctic Ocean is positive; [2]Roach *et al.* (1995); [3]Woodgate *et al.* (2010); [4]Woodgate *et al.* (2006); [5]Woodgate *et al.* (2005); [6]Cuny *et al.* (2005); [7]Curry *et al.* (2011); [8]Smedsrud *et al.* 2010; [9]Skagseth *et al.* (2008); [10]Schauer *et al.* 2008; [11]Rudels *et al.* 2008; [12]Unpublished data of Beszczynska-Möller; [13]deSteur *et al.* (2009); [14]Rabe *et al.* (2009); [15]Schauer & Beszczynska-Möller (2009). [*]heat flux calculated with reference temperature -0.1 [o]C [**]heat flux for closed volume budget (reference temperature arbitrary)[***]heat flux referenced to freezing temperature. *Table modified from Beszczynska-Möller et al. (2011).*

| Gateway | Net Volume Flux (mean for years) | Variability (Sv) | Liquid Freshwater Flux (mSv) | Heat flux (TW = $10^{12}$ W) |
|---|---|---|---|---|
| **Bering Strait** | **1.0 ± 0.2**<br>1.2[1]<br>0.8 ± 0.2 (1990 – 2007) [2,3,4] | Daily –2 to 3 [5]<br>Monthly 0.4 to 1.3[5]<br>Inter-annual 0.6 to 1.0[5] | **-72 ± 14**<br>80 ± 20[4] | **13 ± 2**<br>5.7 ± 2.0[1]<br>10 – 20 [3***] (1998 – 2007) |
| **Davis Strait** | **-3.1 ± 0.7**<br>-2.2[1]<br>-2.6 ± 2.0[6] (1987-1990)<br>-2.3 ± 0.7[7] (2004 – 2005) | | **119 ± 14**<br>-92 ± 34[6] (1987 – 1990)<br>-116 ± 41[7] (2004 – 2005) | **28 ± 3**<br>18.0 ± 3.5[1]<br>18 ± 17[6*] (1987 – 1990)<br>20 ± 9[7*] (2004, 2005) |
| **BSO** | **3.6 ± 1.1**<br>2.5[1]<br>2.0[8,9] (1997 – 2007) | Inter-annual 0.8 to 2.9[9] | **31 ± 13**<br>55 to 60[8] (1997 – 2007) | **86 ± 19**<br>60.5 ± 6.1[1]<br>50[8,9] to 70[9**] (1997 – 2007) |
| **Fram Strait** | **-1.6 ± 3.9**<br>-1.8[1]<br>-2.0 ± 2.7[10] (1997 – 2007)<br>-1.7[11] (snapshots 1980 – 2005) | Monthly -8.4 to -0.2[12]<br>Inter-annual -4.7 to -0.3[12](2002 - 2008) | **110 ± 40**<br>-80 to -66[13,14] (1997 - 2008)<br>-65[11] (snapshots 1980 - 2005) | **62 ± 17**<br>20.9 ± 7.6[1]<br>36 ± 6[15**] (1997 – 2009)<br>29[11](snapshots 1980 – 2005) |
| **Total Advective** | **0.19 ± 4.13**<br>-0.3[1] | | **187 ± 44** | **189 ± 26**<br>105.2 ± 8.9[1] |

### 1.2.3 Mixing in the Arctic Ocean

Diapycnal mixing, which mixes and maintains the stratification in the ocean interior, is driven by intermittent patches of small-scale turbulence caused principally by breaking of internal gravity waves, but also from other processes such as double diffusive processes. This turbulence generates property gradients that are irreversibly removed by molecular diffusion and is caused mainly by changes in atmospheric wind forcing, which creates internal oscillations in the oceanic surface mixed layer, and barotropic lunisolar tidal currents impinging on topography in a stratified ocean. Turbulent mixing is the result of many individual events, intermittent in time and space, and is very spatially and temporally variable as mechanical forcing is highly unsteady.

In the Arctic Ocean the main transformation is towards less dense waters, however the AW layer is transformed into both less dense and denser waters. The large density gradient between the relatively light surface water and the denser AW prevents upwelling of the AW (Rudels *et al.* 1999), and creates boundary interleaving and intrusions where water masses meet.

A modeling study by Zhang & Steele (2007) investigated the sensitivity of the Arctic Ocean to background vertical diffusivity by comparing their model to the Polar Hydrographic Climatology (PHC) data, and concluded that the water properties and circulation are best reproduced using an average diapycnal mixing rate of $10^{-6}$ $m^2s^{-1}$. Larger values were found to weaken the modeled ocean stratification in the Canada Basin and result in anticyclonic circulation at all depths (Zhang & Steele 2007). Fer (2009) found that a vertical mixing rate of 5 x $10^{-5}$ $m^2s^{-1}$ is enough to erode the cold halocline. This is much lower than the value of average oceanic abyssal mixing of $10^{-4}$ $m^2s^{-1}$ inferred from the abyssal ocean's mass and heat balance by Munk (1966), as well as the value of $10^{-5}$ $m^2s^{-1}$ used in most open ocean models (e.g. Large *et al.* 1994).

Microstructure measurements in the Alaskan continental shelf and Amundsen basin found an average diffusivity of 1.4 x $10^{-7}$ $m^2s^{-1}$ (Rainville & Winsor 2008). In the upper ocean (100 – 400 m) the highest diffusivities (2 x $10^{-5}$ $m^2s^{-1}$) are found on the Alaskan shelf. In the deeper ocean and the interior basins typical diffusivities values are of $10^{-6}$ $m^2s^{-1}$, estimated from microstructure observations (Lenn *et al*. 2009). Highly uniform enhanced dissipation is associated with the sharp temperature increase at the top of the AW layer in the western Arctic (200 – 300 m) (Rainville & Winsor 2008), but the Arctic boundary internal wave field can be as low as in the central Arctic (Lenn *et al.* 2011).

The enhanced value at the top of the AW layer is thought to be due to double diffusion (Kelley *et al.* 2003; Woodgate *et al.* 2007), a consequence of the weak internal wave field leading to the formation of thermohaline staircases which link the AW to the cold fresh overlying waters. The staircases arise from the opposing contributions of the temperature and salinity gradients on density and the greatly differing molecular diffusion rates for heat and salt. This region is characterized by distinct thin strong gradient layers where the heat transfer is provided by molecular diffusion in the strongly stratified laminar interfaces and by turbulent convective mixing in the well-mixed homogeneous layers. Well-defined staircases and diffusive convection has been observed in the central Arctic (Neshyba *et al.* 1971, Melling *et al.* 1984, Padman & Dillon 1987, 1988, Timmermans *et al.* 2008) and in the Arctic boundary current (Lenn *et al.* 2009, Polyakov *et al.* 2011). Sirevaag and Fer (2012) found significant splitting and merging of the staircases in the Amundsen basin, indicating additional processes besides double-diffusive mixing are taking place. The small double diffusive fluxes mean that the deep waters are essentially isolated from the layers above (Timmermans & Garrett 2006).

Intrusions are also observed across the Arctic Ocean, for example in the Eurasian Basin (e.g. Rudels *et al.* 1999; May & Kelley 2001; Dmitrenko *et al.* 2008). These are probably

caused by the strong lateral temperature gradients in the AW inflow regions, and can contribute to heat transfer towards the surface through double diffusive convection (Rudels *et al*. 1999; McLaughin *et al*. 2009).

Tides are generally weak in the Arctic Ocean. Most of the Arctic is situated poleward of the tidal critical latitude (74.5 $^{o}$ N) beyond which the rotation of the earth prohibits freely propagating waves at the dominant semidiurnal ($M_2$) tidal frequency. Tidally generated waves at these latitudes have short temporal and spatial scales related to the local topography and stratification and are dissipated rapidly leading to local turbulent mixing (Watson *et al.* 2013) and large variability in dissipation (Lenn *et al.* 2011). Simmons *et al*. (2004) concluded that, with the exception of hot spots and although locally important, internal wave energies generated from tidal interactions are small compared to low latitude levels. Over the broad European shelf seas typical tidal velocities of 5 – 15 cms$^{-1}$ are found (Kowalik & Proshutinsky 1993, Figure 4), which is enough to generate internal waves over suitable topography. Values of more than 50 cms$^{-1}$ are found near Bear Island on the western Barents Sea, south of Svalbard (Kowalik & Proshutinsky 1995, Padman & Erofeeva 2004), and in the southern Barents Sea near the entrance to White Sea. Strong (>20 cm/s) currents are found in Davis strait in the Labrador sea and in Nares strait, and in various location within the CAA. Currents are weak over the deep basins and along the northern coast of Alaska (Padman & Erofeeva 2004).

Wind acting on the sea surface creates a direct conversion of energy from the atmosphere to the ocean, which is mostly limited to the surface mixed layer of the ocean (Wunsch & Ferrari 2004), but a fraction can propagate deeper in the water column and contribute to vertical mixing (Ferrari & Wunsch 2009, Alford 2010). Various 2-D numerical models show that winds have an effect on Arctic Ocean circulation (Ponomarev & Fel'zenbaum 1975, Proshutinsky 1988, 1993). These models attribute variations in surface circulation

(both of sea and ice) to wind fields, both at seasonal and year to year time scales. Sea ice cover reduces internal wave energy production by damping and energy dissipation (Levine *et al.* 1985; D'Asaro & Morison 1992), despite the possible enhanced forcing due to ice mobility. Ekman transport, or the movement of surface waters in response to wind, can cause upwelling of deeper water by convergence or divergence. Upwelling of AW has been observed (e.g. Aagaard & Roach 1990) and inferred (Woodgate *et al.* 2005) in the northern Chukchi Sea and linked to wind forcing.

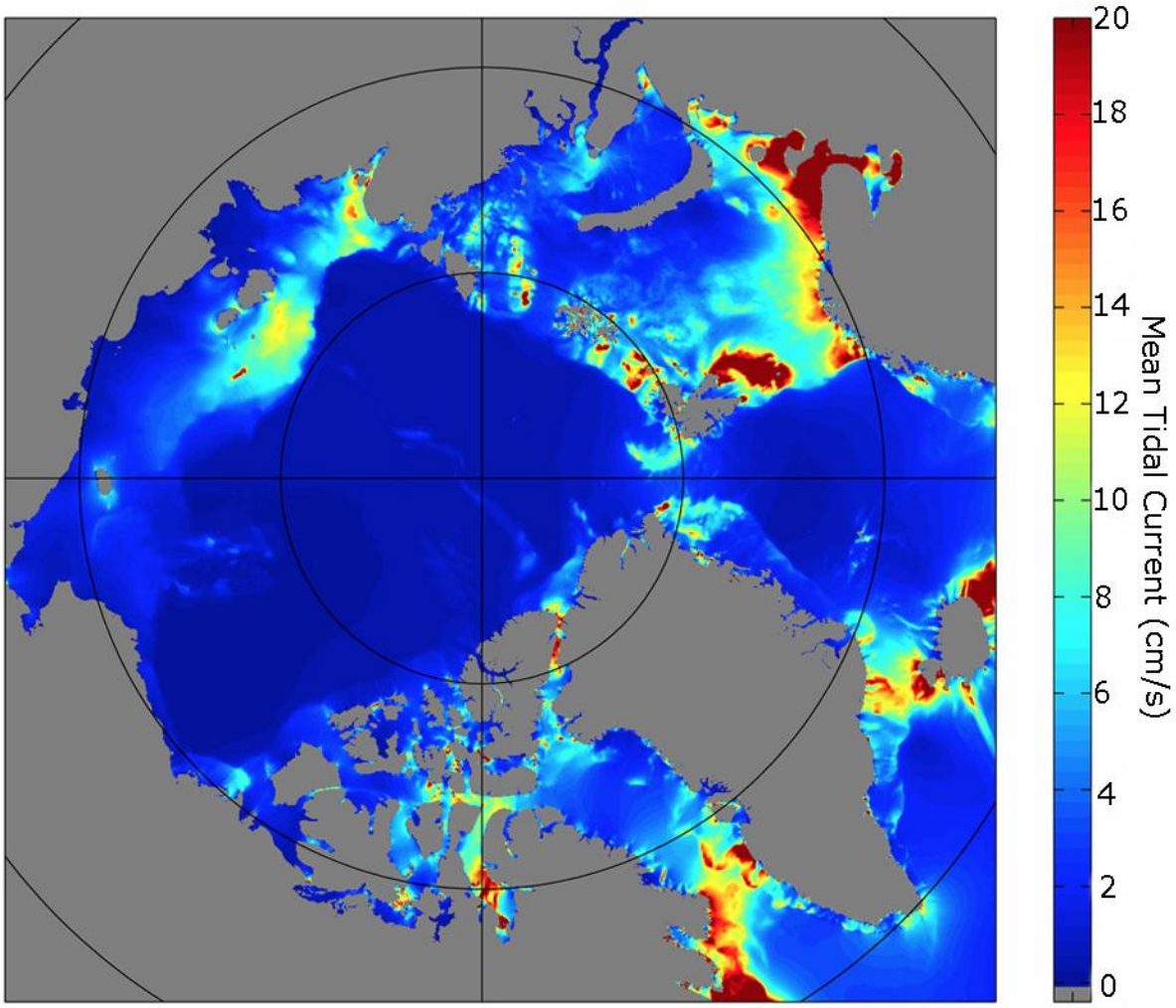


**Figure 4:** Mean tidal current speed ($cms^{-1}$) based on simulating 14 days of hourly total tidal speed using an inverse model (Padman & Erofeeva 2004).

Other sources that may power turbulence in the ocean are: heating and cooling by the atmosphere or surface buoyancy forces, exchange of freshwater with the atmosphere, geothermal heating through the sea floor and atmospheric pressure loading. These are negligible in net energy input when compared with tides and winds, and except for geothermal heating, confined to the upper ocean (Wunsch & Ferrari 2004).

### 1.2.4 Dense Water Formation in the Arctic

The imported warm saline AW increases significantly in density as it circulates around the Arctic due to atmospheric cooling and ice formation (Mauritzen 1996). The rate of this transformation is estimated at 6.5 ± 0.7 Sv (Lumpkin & Speer 2003), contributing to global dense water. Some of this deep water is likely formed in the vast shallow shelves of the Arctic as dense, brine-enriched waters are drained off the shelves entraining water as they sink. This process is known as slope convection and is an intermittent process, regionally confined to the Barents, Kara and Laptev seas. It is conditioned by the meteorological and hydrographic environments of the shelf seas and their bathymetry (Aagaard *et al.* 1985; Rudels 1986; Rudels *et al*. 1994, Shapiro *et al.* 2003).

Martin & Cavalier (1989) estimate that 20 to 60 % of the Arctic dense water is formed in the polynyas on the Siberian shelf, due to ice production and brine rejection. The rate of bottom water (>1500 m) renewal is affected by the Lomonosov Ridge, with a renewal time of 30 years in the Amundsen and Nansen Basins but 700 years in the Canada and Makarov Basins (Östlund *et al.* 1987).

### 1.2.5 Seasonality in the Arctic Ocean & Long-term Variability

The internal wave environment is expected to be very different in summer and winter due to varying forces and stratification. The integrated average dissipation rate of baroclinic tidal energy is ~9.2 x $10^{10}$ W in summer and ~3.1 x $10^{10}$ W in winter (Kagan *et al.*

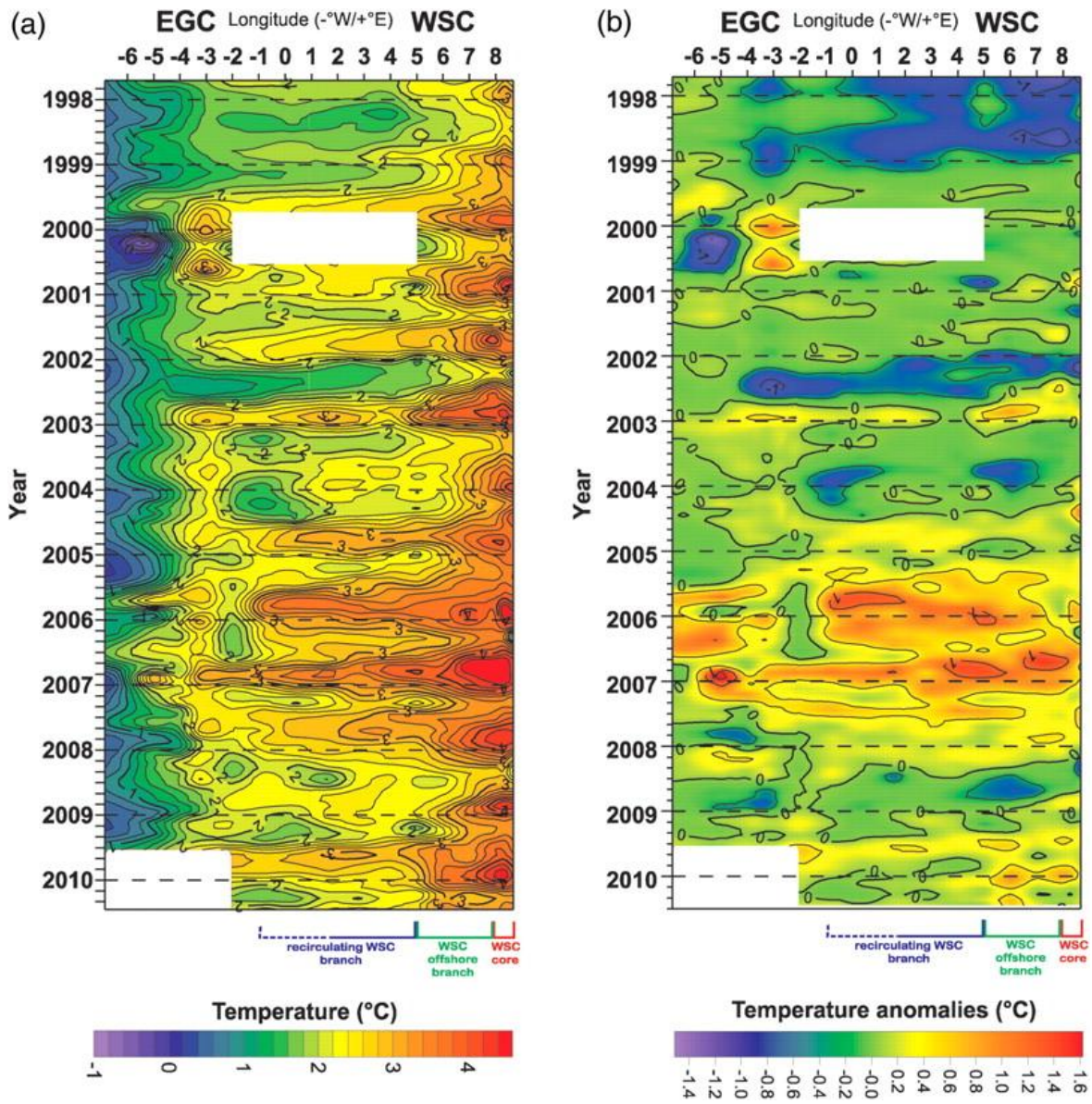


**Figure 5:** Spatio-temporal diagram of monthly means of (a) Temperature at 250 m and (b) Temperature anomalies from a monthly cycle (calculated about the mean seasonal cycle), measured from the East (East Greenland Current, EGC) to the west (West Spitsbergen Current, WSC) across Fram Strait (Beszczynska-Möller *et al.* 2012).

2010).There is a large seasonal discrepancy in wind force between summer and winter (Yang & Comiso 2007). In winter strong convection and storms are expected, with evidence of enhanced near-inertial motion (Merrifield & Pinkel 1996). Large areas of open water in summer and loose pack ice are expected to create wind driven near-inertial motion

(Plueddemann *et al.* 1998, Rainville & Woodgate 2009). Summer warming by increased solar radiation is very small and mostly lost to ice melting, therefore the seasonal increase in heat is caused by advection of warmer Pacific water and AW.

The Arctic Ocean is known to vary greatly on an inter-annual to decadal time scale. Figure 5 by Beszczynska-Möller *et al.* (2012) shows the spatio-temporal variability in Fram Strait from 1998 to 2010 at a depth of 250. Two distinct periods of temperature increase can be seen. The first period runs from 1998 to 2000, and the second one starts in 2004 and lasts till 2008. The latter, at its peak in September 2006, produced temperatures of > 3 $^{o}$C higher than the mean in the east of Greenland. Since the boundary CTD data used for estimating the volume flux field at the openings of the Arctic was collected during the start of the second of these warming events (2005), it might not be fully representative of the average Arctic Ocean conditions. This is especially significant since the Polar Hydrographic Climatology (PHC) data, used for estimating the conditions in the interior of the Arctic, is heavily weighted toward the 1970's and 1980's when the Arctic Ocean was probably in a colder state (Polyakov *et al*. 2004).

# 2. Theory and Method

## 2.1 Introduction

The relationship between buoyancy exchanged by mixing and upwelling of fluid within the abyssal ocean is described by the advection-diffusion equation (Munk 1966). This is based on the concept that water entering an enclosed basin (the Arctic Ocean) from adjacent sources can only leave this basin at a different density than it entered through mixing, or by sources and sinks. This mixing can be quantified using an Advection-Diffusion Balance which states that, over an ocean basin, the diapycnal mixing required to maintain the density stratification can be calculated assuming that there is a balance between horizontal advection in and out of the basin (volume flux data at boundaries of the basin), and vertical mixing between isopycnal layers (parameterized by a diapycnal mixing coefficient).

Based on this geometry, a simple box model of the Arctic Ocean, divided into a series of 16 potential density layers (referenced to the sea surface, $\sigma_0$), was constructed. The seabed is the base and the sea surface is the lid of the model, and the sides are completely enclosed by coastline except for Fram Strait, Davis Strait, BSO and Bering Strait, where hydrographic data are available. The only other opening from the Arctic is the Fury & Hecla Strait in the CAA, which is partially blocked and very narrow (~ 5 km length in total) at the eastern end where it connects to the Atlantic Ocean through the Labrador Sea. As there are no adequate measurements available to resolve its volume flux, which is estimated to be negligible by Tsubouchi *et al*. 2012 (~5 mSv), this strait was ignored.

The rates of transformations within the Arctic Ocean were estimated based on the volume flux data by Tsubouchi *et al.* (2012), along sections at these four openings of the Arctic and assumed to represent the flow field of the whole Arctic (Figure 1).

The volume flux at the boundaries of the basin was calculated using a mass balance equation, which is explained next in this section. Then the advection-diffusion equation and the equations used to calculate the dissipation are listed, as well as their assumptions. Finally the data and the model used are described.

## 2.2 Mass Balance Equation

The net ocean flux through the side of the volume, v, can be calculated using the mass (volume) balance equation, which states that:

$$\mathrm{v} = \oint u dA \tag{1}$$

Where $u = u\,(s, z)$ is the distribution of ocean velocity normal to the sides of the volume, $s$ is the along-side distance coordinate and $z$ is the vertical (depth) coordinate. $A$ represents the side area and $dA = dsdz$ is an area element. For each strait, the volume flux corresponding to the water mass layer was found and summed in order to find the total volume flux of that layer.

The volume conservation equation is allowed as long as an unfeasibly short time scale is not used. This was estimated as ~6 days by using barotropic wave propagation speeds to approximate the adjustment time scale over which stationarity may be assumed (Tsubouchi *et al*. 2012). The hydrostatic and geostrophic balance assumptions are applied to the inverse model. The hydrostatic balance assumes that the vertical pressure gradient is in a perfect balance with density, and holds on regional scales. The geostrophic balance states that the horizontal pressure gradients in the ocean almost exactly balance the Coriolis force resulting from horizontal currents. This is true within the ocean interior away from the top and bottom Ekman layers, and large spatial (> 50 km) and temporal (> days) scales. The geostrophic balance also requires that viscosity and the non-linear terms in the equation of motion are negligible. The nonlinearities in the equation of state are responsible for the

temperature and pressure dependence of density and can give rise to internal energy changes. These effects are assumed to be very small compared with the total uncertainty of the model, and therefore play only a minor role in large-scale ocean processes.

### 2.3 The Advection-Diffusion Balance

If a system is in steady state balance between horizontal advection of density and vertical diffusion, the vertical mixing required to maintain the density stratification can be explained using:

$$\nabla \cdot (U\sigma_0) = -\nabla \cdot (K\nabla\sigma_0) \tag{2}$$

Where $U = (u, v, w)$ is the velocity field and $u$, $v$, and $w$ are the zonal, meridional and vertical components of velocity, $\sigma_0$ is the potential density referenced to zero and $K$ is turbulent eddy diffusivity. Surface fluxes are ignored. The volume integral of (2) over an ocean layer can be calculated by applying the divergence theorem, which states that in the absence of sources or sinks, the volume, $V$, of a body of fluid within a region can only change as a result of a flow though its boundary, using:

$$\oiint (U\sigma_0) \cdot dA = -\int (K\nabla\sigma_0) \cdot dA \tag{3}$$

For an ocean layer bounded by isopycnal surfaces in a coordinate system with $(x, y, z)$ = *(east, north, upward),* the one-dimensional linear advection-diffusion balance for a conservative scalar property of a fluid, assuming that there are no sources or sinks is:

$$\oiint \mathrm{v}\sigma_0 dA = (F^u - F^l) + ({\sigma_0}^u W^u) - ({\sigma_0}^l W^l) \tag{4}$$

Where $l$ and $u$ superscripts represent the lower (denser) and upper (lighter) surface bounding an isopycnal layer and the vertical integration runs from the depth corresponding to ${\sigma_0}^l$ to the depth of ${\sigma_0}^u$over quasi-horizontal density surfaces. $F$ is the diabatic diffusive transport of potential density. (Equations modified from Huussen *et al.* 2012).

The vertical advective transport of volume, *W*, can be found from the vertical velocity *w*, where $W = \iint w(x,y)dxdy$, and *w* follows from the continuity equation:

$$\iint \mathrm{v}(x,z)dxdz + \iint w^{l}(x,y)dxdy - \iint w^{u}(x,y)dxdy = 0 \quad (5)$$

*F* can be related to the turbulent diffusivity *K* using,

$$F = \overline{K\sigma_{0_z}}\, A \quad (6)$$

*K* is the parameterization of the mixing processes leading to a diapycnal buoyancy flux. The over-bar indicates spatial averaging over surface area and $\sigma_{0_z}$ is the vertical density gradient. Horizontal averaging of *K* over broad regions works reasonably well in the ocean interior because isopycnals are dominantly horizontal away from topography, but *K* is ill-defined in the absence of stratification.

The Advection-Diffusion equation assumes the magnitude of horizontal motion to be much larger than vertical motion. The steady state condition does not allow for time variation of the model result and results in a single-view, basin-average mixing rate of the Arctic fluxes resulting from a multitude of events and processes of different time and length scales that might not be representative of the long-term displacements, and does not distinguish between interior and boundary values.

The calculation was done starting with the bottom layer. At the seafloor the vertical advective and diffusive transport is assumed to be zero ($F^{l} = 0$ and $W^{l} = 0$). Since the bottom layer lies at a depth deeper than ~ 1000 m, it can only communicate with the outside of the Arctic basin through Fram Strait (Figure 6). Therefore, by taking the volume flux data for the bottom layer at Fram Strait and integrating (4) from the seafloor upwards, the vertical diffusive flux of potential density at the top interface of this bottom layer can be solved. The vertical transport through the upper density interface $W^{u}$ was calculated from continuity (5). This value was then used to calculate the vertical mixing for the next layer, and so on.

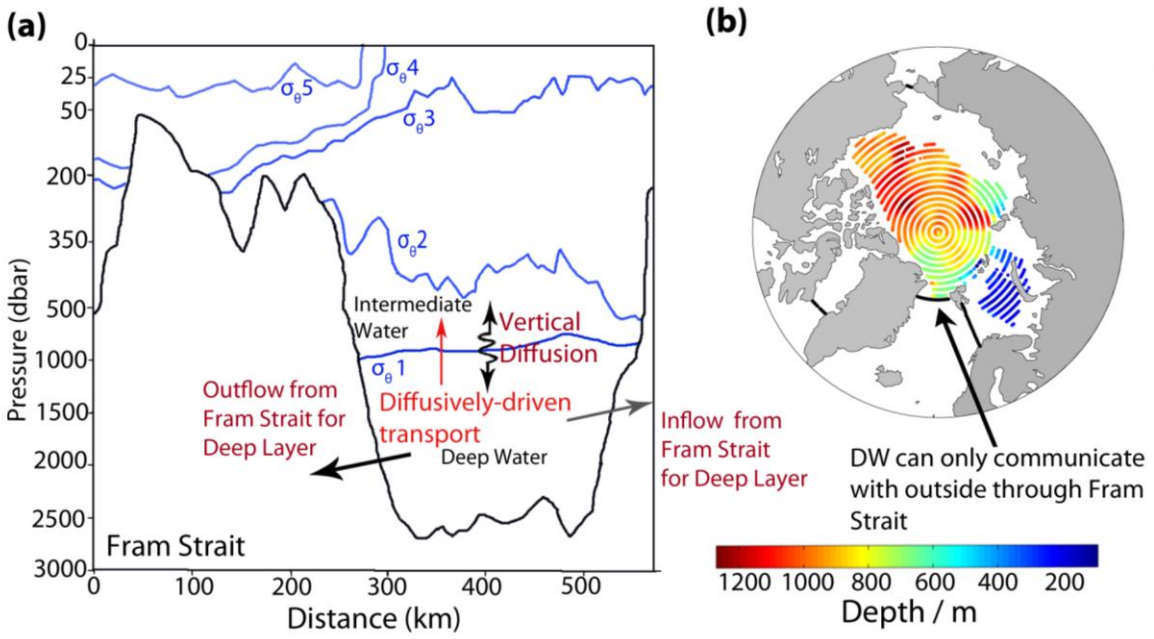


**Figure 6:** (a) Schematic zonal cross-section of Fram Strait showing the isopycnal model layers and the horizontal flow across the strait. (b) Spatial distribution of the bottom layer (Deep Water; DW), showing the depth to this layer interface based on PHC climatology (Steele *et al.* 2001).

The relative error of the large-scale layer transport is assumed to be equal to the inverse model errors in Tsubouchi *et al.* 2012, which is an a priori uncertainty in the reference velocities as the standard deviation of moored velocity data (~ 0.02 – 0.05 m/s) leading to an uncertainty in the volume conservation of ~1 Sv for the full depth transport decreasing from higher in the upper layers (~4 Sv) to lower in the deeper layers (~0.5 Sv). Errors also result from using potential density and from the interpolation.

## 2.4 Estimating dissipation and power required to sustain mixing

To calculate the energy required to sustain the mixing, $\overline{\sigma_{0_z}}$ and $\overline{K}$ in (6) are averaged out assuming they are spatially uncorrelated, such that $\overline{K\sigma_{0_z}} = \overline{K} \times \overline{\sigma_{0_z}}$ (Polzin *et al.* 1995). Osborn (1980)'s simple mixing model is then used to relate the mixing rate to the rate of turbulent kinetic energy dissipation, by assuming a constant mixing efficiency. This model

states that the viscous diffusion coefficient ($\epsilon_T$ in W/kg), driving a downward buoyancy flux ($KN^2$), is equivalent to the work done against gravity by the turbulent mass transport to raise the center of mass and thus the background potential energy, and can be calculated from:

$$\epsilon_T = K\frac{N^2}{\Gamma} \tag{7}$$

Where $\Gamma$ is the mixing efficiency, $N$ is the buoyancy frequency and is a measure of the stratification:

$$N = -\sqrt{\frac{g}{\rho_R}\sigma_{0_z}} \tag{8}$$

and $g$, and $\rho_R$ are the gravity and reference density constants respectively.

The mixing efficiency is defined as the fraction of the energy of breaking internal waves available to mix the fluid, with the rest of the energy being dissipated by viscous friction and heat. A canonical value for $\Gamma$ of 0.2 is typically used for shear flows (Peltier & Caulfield 2003).

Equations (6), (7) and (8) can be simplified into:

$$\epsilon_T = \frac{F}{A}\cdot\left(\frac{1}{\Gamma}\cdot\frac{g}{\rho_R}\right) \tag{9}$$

This equation was initially used to calculate the diffusion coefficient. However, open ocean observations show a varying $\Gamma$ with observations commonly 0.15 – 0.25 (Toole *et al*. 1994, Ledwell *et al*. 2000), whilst indirect (Stigebrandt & Aure 1989) and theoretical estimates (Arneborg 2002) have suggested a lower value of $\Gamma$ = 0.05 – 0.1. In the low turbulence environment of the Arctic the assumption of local isotropy become doubtful and a constant mixing efficiency of 0.2 is likely an overestimate. In order to find a more accurate value for the diffusion coefficient, the equations developed by DeLavergne *et al.*

(2015) were used. They use empirical measurements to suggest that the dissipation coefficient can be calculated from:

$$K = \frac{4 \cdot \sqrt{(1 - \Gamma)\epsilon_T \cdot v}}{N} \tag{10}$$

Where *v* is the molecular kinematic viscosity of seawater.

According to (10), increasingly strong turbulence intensities lead to higher mixing efficiencies, which means that as turbulence grows inhibited by stratification it becomes increasingly inefficient at driving a buoyancy flux. The calculation is carried out ignoring the top two layers as these are considered the mixed layer.

The power required to achieve the calculated diffusion is then calculated by bottom-up integration of the dissipation rate with depth and multiplied by the area:

$$P \approx \sum \epsilon_T \, \rho_R \, A \, \Delta z \tag{11}$$

Where Δz is the mean layer thickness.

## 2.5 Model Layers

The density boundaries for the subdivision of the water column were based on the density criteria from Rudels *et al.* (2008). Six main water masses are used: Surface Water (SW), Subsurface Water (SSW), Upper Atlantic Water (UAW), AW, Intermediate Water (IW) and Deep Water (DW), which were further subdivided to 16 layers to increase the model resolution (Table 2).

Potential density referenced to the sea surface ($\sigma_0$) was used throughout this study in order to consistently conserve mass within layers since mass flux is being used. This only approximates surfaces along which water parcels flow adiabatically. Software to approximate neutral density, a more appropriate form of density surface, is not available for the Arctic Ocean. The $\sigma_0$ surface was converted from the potential density surfaces

referenced to various depths by Tsubouchi *et al.* (2012) using the Bisection Method. This is a simple root-finding solution for an equation with a single solution lying between two definable boundaries. It runs by repeatedly bisecting the interval and determining which half contains the solution and re-running using this method until a sufficiently small interval is found in which to estimate the root. Table 2 shows the difference between these two depths and the resulting root-mean-square deviation of the depth difference.

Figure 7 shows the depth and topography of the layer interfaces for the main water masses. The most striking feature, especially at shallower isopycnals, is the Beaufort Gyre. This is seen as a circular deepening of the isopycnals in the Beaufort Sea (Figure 7a, b) and is due to strong anticyclonic wind stress curl caused by the Beaufort Sea High (Proshutinsky *et al.* 2009). This influence decreases with depth, and at the interfaces between the Upper AW and the AW (UAW/AW), the AW and the Intermediate Water (AW/IW), and the Intermediate Water and the Deep Water (IW/DW) the shape of the isopycnals appears to be less affected by the gyre and broadly related to the topography. At the interfaces of the Subsurface layer and the Upper AW layer (SSW/UAW) and the UAW/AW, the input of the Lomonosov Ridge can be seen as a sharp gradient approximately north-south across the centre of the Arctic Ocean (Figure 7b, c).

Both the SW/SSW and SSW/UAW interfaces outcrop at the sea surface in the Barents Sea, with the densest surface outcrop being $\sigma_0 \sim 27.63$ (Figure 7c).

**Table 2:** Definitions of model layer interfaces, the water mass name and their mean depth. The $\sigma_0$ surface used in this work, and the equivalent interface defined by Tsubouchi *et al.* (2012) are listed, including the difference in mean depth between these two and their standard deviation error.

| **Water Mass** | **Interface** | **$\sigma_0$** | **Defined by Tsubouchi 2012** | **Mean depth (m)** | **Difference between depth** | **Std. dv.** |
|---|---|---|---|---|---|---|
| SURFACE WATER (SW) | 1. SW (1) /SW(2) | 24.700 | 24.700 ($\sigma_0$) | 23.8 | 0 | 0 |
| | 2. SW (2)/ SW (3) | 25.500 | 25.500 ($\sigma_0$) | 42.6 | 0 | 0 |
| | 3. SW (3)/ SSW(1) | 26.000 | 26.000 ($\sigma_0$) | 57.8 | 0 | 0 |
| SUB SURFACE WATER (SSW) | 4. SSW(1)/SSW(2) | 27.000 | 27.000 ($\sigma_0$) | 95.2 | 0 | 0 |
| | 5. SSW(2)/UAW(1) | 27.100 | 27.100 ($\sigma_0$) | 100.4 | 0 | 0 |
| UPPER ATLANTIC WATER (UAW) | 6. UAW(1)/UAW(2) | 27.300 | 27.300 ($\sigma_0$) | 111.3 | 0 | 0 |
| | 7. UAW(2)/AW(1) | 27.500 | 27.500 ($\sigma_0$) | 138.7 | 0 | 0 |
| ATLANTIC WATER (AW) | 8. AW(1)/AW(2) | 27.600 | n/a | 158.9 | n/a | n/a |
| | 9. AW(2)/AW(3) | 27.700 | 27.700 ($\sigma_0$) | 193.0 | 0 | 0 |
| | 10. AW(3)/IW(1) | 27.921 | 30.280 ($\sigma_5$) | 296.7 | 2.62 | 0.22 |
| INTERMEDIATE WATER (IW) | 11. IW(1)/IW(2) | 27.948 | n/a | 339.8 | n/a | n/a |
| | 12. IW(2)/IW(3) | 27.962 | 30.320 ($\sigma_5$) | 384.1 | 1.93 | 0.31 |
| | 13. IW(3)/DW(1) | 28.037 | 32.750 ($\sigma_1$) | 841.4 | -4.52 | 0.53 |
| DEEP WATER (DW) | 14. DW(1)/DW(2) | 28.076 | 35.126 ($\sigma_{1.5}$) | 1501.3 | -44.18 | 3.83 |
| | 15. DW(2)/DW(3) | 28.087 | 35.142 ($\sigma_{1.5}$) | 1842.5 | -24.77 | 5.26 |

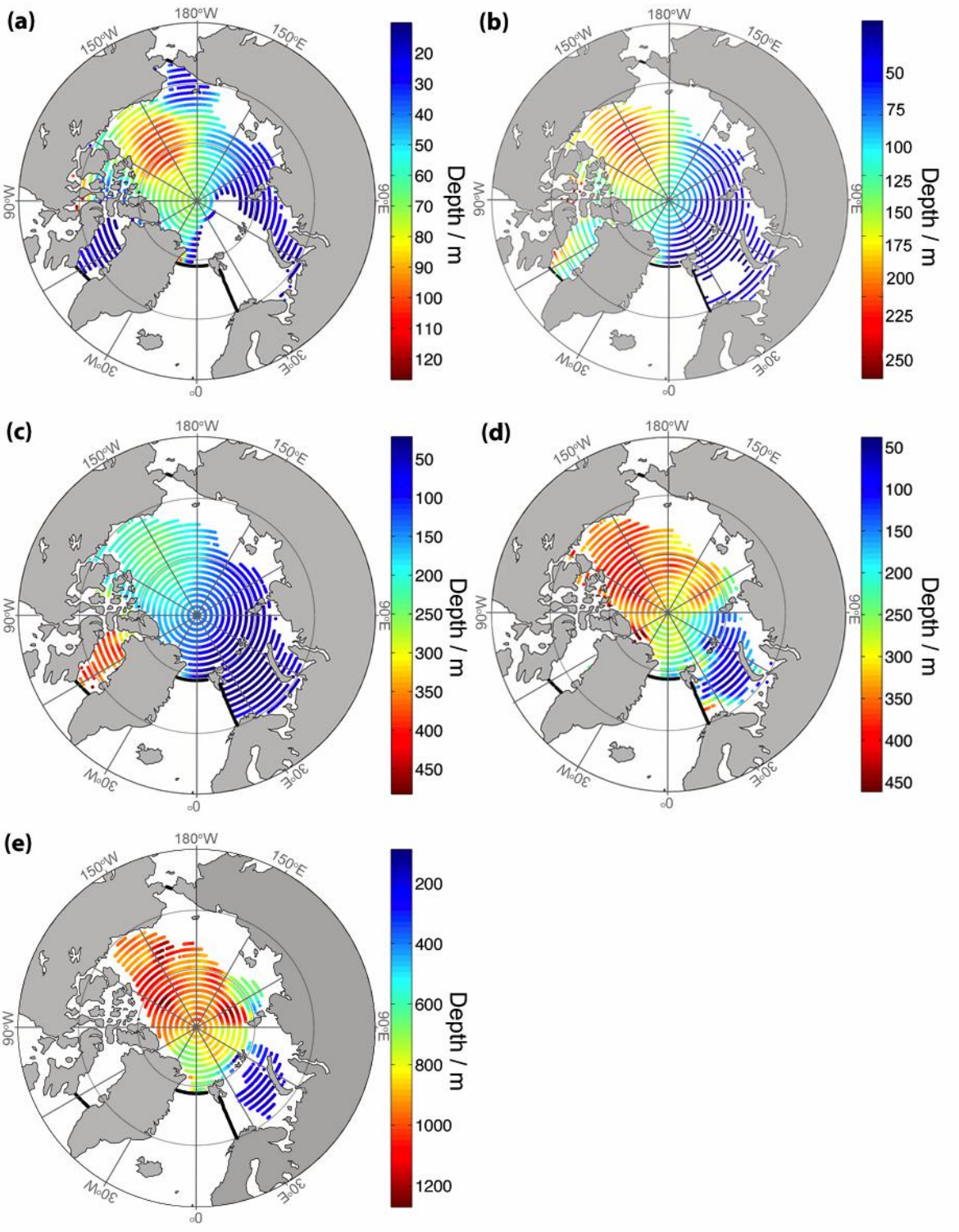


**Figure 7:** Maps showing depth to, and topography of, the isopycnal layer interfaces defined in this project. (a) – SW/SSW; (b) – SSW/UAW; (c) – UAW/AW; (d) – AW/IW; (e) – IW/DW. Plots made using PHC Summer mean climatology data set (Steele *et al.* 2001).

## 2.6 Data & Data Quality

The data used to define the properties of the layer interfaces is the PHC (Polar science center Hydrographic Climatology) data set (Steele *et al.* 2001), which contains a mean climatology for Summer (July –September), with in-situ temperature and salinity data at 1 x 1 degree intervals for incremental depth levels down to 5500 m (Table 3). This climatology is the result of merging the World Ocean Atlas (WOA, Levitus) 1998, the EWG Arctic Ocean Atlas (AOA) and Canadian data provided by the Bedford Institute of Oceanography (BIO) using optimal interpolation technique.

Hydrographic observations in the four main gateways of the Arctic – Davis, Fram, and Bering Straits, and the BSO, and moored arrays of current meters for summer (August – September) 2005 were used to calculate the volume flux through the Arctic boundaries (Tsubouchi *et al.* 2012). These consist of 131 finely spaced hydrographic stations at the boundaries and 16 GCM grid cells in the BSO, which function as CTD stations in regions of absent data. The observational data consists of 16 stations in Davis Strait (Lee *et al.* 2004), 74 stations in Fram Strait (Fahrbach & Lemke 2005), 29 stations in the BSO (Skagseth *et al.* 2008), and 12 stations in the Bering Strait (Woodgate *et al.* 2005). The model used is an implementation of the Nucleus for European Modeling of the Ocean (NEMO) coupled ice-ocean GCM at NOC Southampton (Barnier *et al.* 2006). The velocity data is measured from 31 moorings deployed in the gateways (full description of data in Tsubouchi *et al.* 2012 and references therein).

**Table 3:** Description of PHC data (Steele *et al*. 2001) showing the main two sources for this data, the WOA and AOA, and their properties.

| | **WOA (*Antonov et al. 1998, Boyer et al. 1998)*** | **AOA *(EWG 1997, 1998)*** |
|---|---|---|
| **Spatial coverage** | Global | 65°N – 90°N |
| **Temporal coverage** | 1900 – 1994 | 1950 – 1989 |
| **Horizontal resolution** | 1° x 1° latitude/longitude grid | 50 km Cartesian grid (Lambert projection) |
| **Depth levels (m)** | 33 total: 0, 10, 20, 30, 50, 75, 100, 125, 150, 200, 250, 300, 400, 500, 600, 700, 800, 900, 1000, 1100, 1200, 1300, 1400, 1500, 1750, 2000, 2500, 3000, 3500, 4000, 4500, 5000, 5500 | 23 total: 0, 5, 10, 15, 25, 50, 75, 100, 150, 200, 250, 300, 400, 500, 750, 1000, 1500, 2000, 2500, 3000, 3500, 4000, 4400 |
| **Climatological means** | Annual, seasonal & monthly. | Seasonal |
| **Data** | *In situ* temperature, salinity | Potential temperature & salinity |
| **Original profile data available?** | Yes | Some |

# 3. Results

## 3.1 Summary of Properties of Defined Model Layers

Figure 8 illustrates the main results, showing the surface area, the density gradient, the vertical velocity, the diabatic diffusive transport and the apparent turbulent diffusivity. These are plotted against layer interface and against a scalar density scale, in order to illustrate the changes in the ocean column. The properties of the upper 100 m surface water layers are approximately homogenous with a sharp change into the AW layer. These results will be explained in detail during the rest of this chapter.

## 3.2 Volume Flux between Model Layers

The calculated volume flux through the boundaries agree with those of Tsubouchi *et al.* (2012), as described in Section 1.2.2.2. Figure 9 shows the total horizontal volume flux for each water mass, calculated during this project as a sum of the flow through the four ocean strait openings. From this figure it can be seen that the SW and DW volume fluxes are negligible. The dominant transport is in the AW layer with an accumulated volume transport of +3.37 Sv. It is balanced by an overall water export in the overlying SSW and UAW, and the underlying IW. Therefore the AW is expected to flux water into the adjacent layers within the Arctic Ocean, transferring water into the surface layers above it and the IW layer beneath it. Tsubouchi et al. (2012) estimated that 2.8 Sv of AW is transported diapycnally within the Arctic, 1.9 ± 1.7 Sv downwards into the IW and 0.8 ± 3.1 Sv upwards into the UAW layer.

The Deep Water layer in Fram Strait is approximately balanced. For the top 1000 m of the basin (above the Deep Water layer), the total Arctic inflow is +9.2 Sv and the outflow is -9.3 Sv. This leaves a deficit of -0.14, which Tsubouchi *et al* (2012) has successfully

balanced by a surface liquid FW flux inflow of +0.19 Sv and sea ice export from Fram strait of -0.05 Sv.

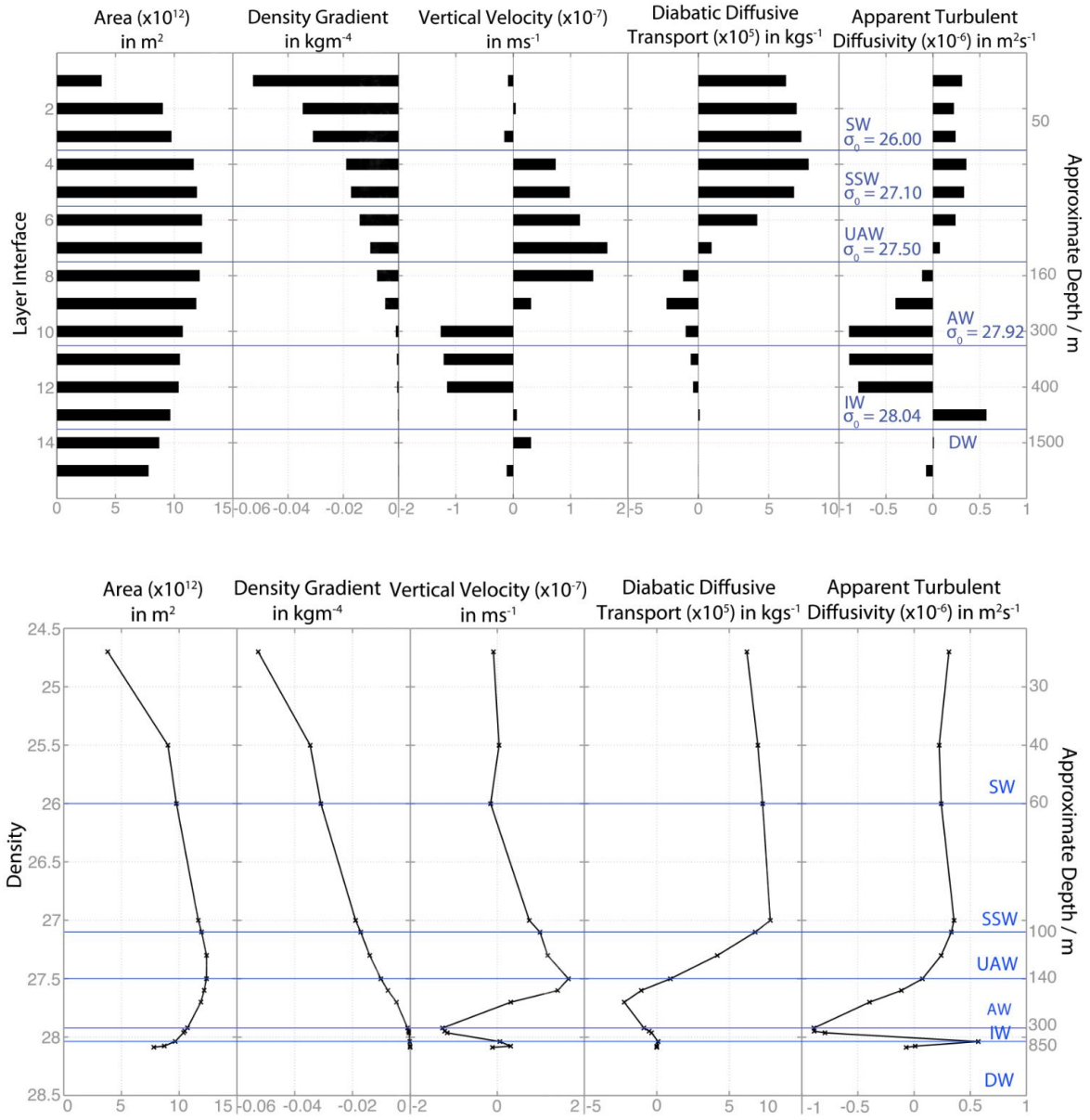


**Figure 8:** Summary of the water properties for each layer interface plotted as the surface area, the density gradient, the vertical velocity, the diabatic diffusive transport and the apparent turbulent diffusivity against (top) layer interface and (bottom) density.

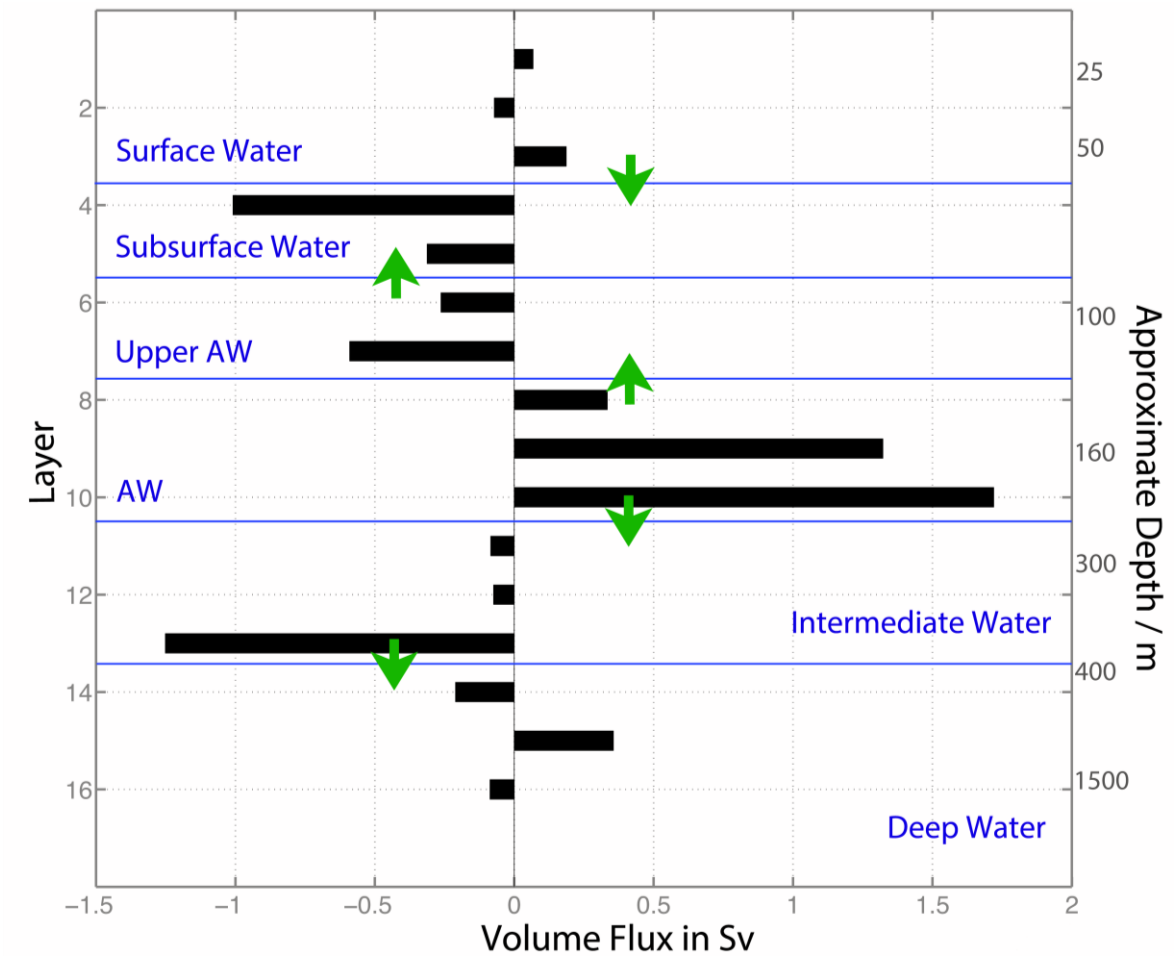


**Figure 9**: Diagram showing the total volume flux for each water mass in the Arctic Ocean in Sv. Arrows indicate the inferred direction of the vertical flux. The defined water masses are labeled.

### 3.3 Density Gradient

The mean density gradient for each isopycnal layer interface was calculated by finding the slope of the regression line for density over a depth range of 10 m above and 10 m below the interface. Areas where the data points were not present, for example if the model layer was thinner than 20m or where the sea surface was less than 10 m above the interface depth, were not included in this calculation. The dz size of 20 m was chosen as the one

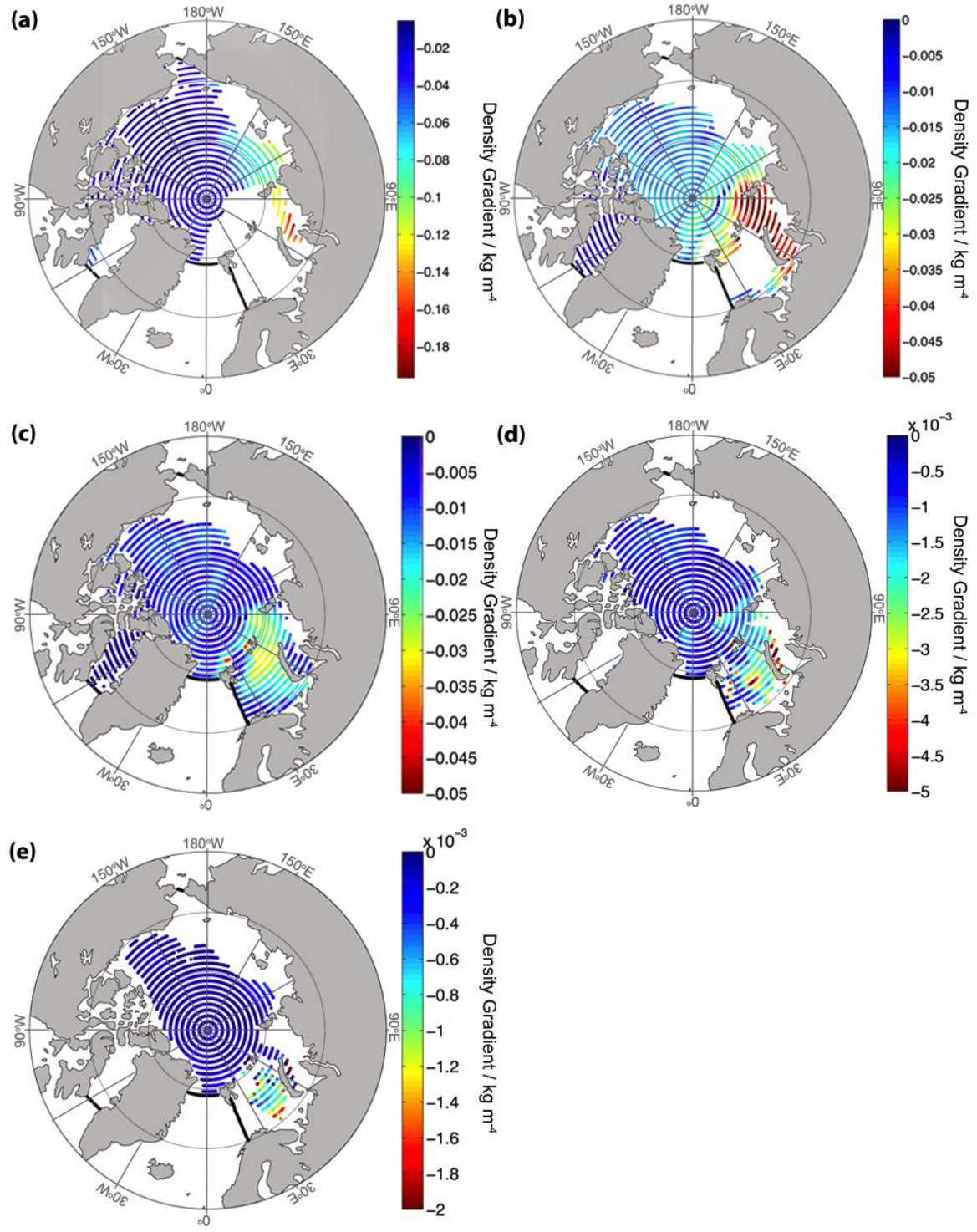


**Figure 10:** Density gradients (in $kgm^{-4)}$ for dz = 20 m at each isopycnal layer ($\sigma_0$) interface, (a) – SW/SSW; (b) – SSW/UAW; (c) – UAW/AW; (d) – AW/IW; (e) – IW/DW..

giving the smallest average density gradient whilst also including a high proportion of the data points.

Figure 10 shows the density gradient for every layer interface. The average density gradient decreases approximately exponentially with1 depth from a value of -0.03 in the SW layer to $-5.02 \times 10^{-5}$ in the DW layer. The density gradient appears to correspond with the Arctic Ocean topography, with low values close to zero in the Canada Basin and Baffin Bay and higher values in Kara Sea and Barents Sea. A large density gradient (approx. - 0.05) can be seen in the Kara Sea in the SSW/UAW interface (Figure 10b), coinciding with an area of enhanced cooling of the AW layer (Dmitrenko *et al.* 2014).

### 3.4 Vertical Velocity

The vertical velocity *w* is positive upward and is equivalent to a diapycnal velocity, as isopycnals are approximately flat in the Arctic and are assumed not to change in thickness with time.

An average velocity of $10^{-7}$ $ms^{-1}$ was found. The dominant diapycnal velocity is seen in the AW layer as $1.4 \times 10^{-7}$ $ms^{-1}$ towards the UAW layer and $-1.2 \times 10^{-7}$ $ms^{-1}$ towards the IW layer (Figure 11), suggesting the AW layer is transferring water into both its adjacent layers.

The area-averaged vertical velocity across the upper AW surface found by Tsubouchi *et al.* 2012 is $1.1 \pm 4.1 \times 10^{-7}$ $ms^{-}$, equating to an export of $0.8 \pm 3.1$ Sv from the AW layer into the UAW layer. The downward velocity across the lower AW surface was calculated by Tsubouchi *et al*. (2012) as $3.1 \pm 2.8 \times 10^{-7}$ $ms^{-1}$, which is equivalent to a downward transport of $1.9 \pm 1.7$ Sv into the IW. The SW and DW layers have negligible velocities of the order of $10^{-8}$ $ms^{-1}$.

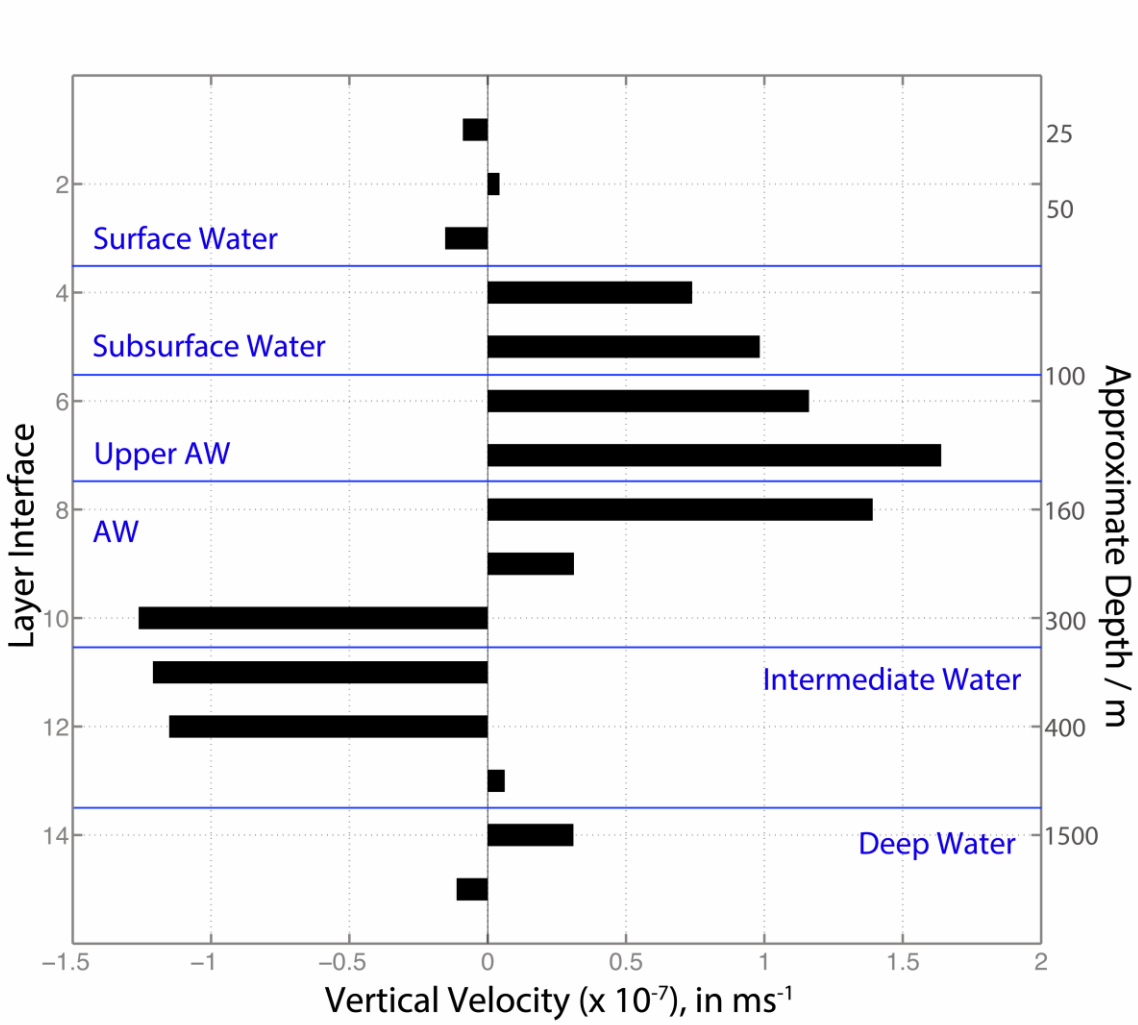


**Figure 11:** Vertical velocity *w* at layer interfaces, where the sign convention is positive upwards. The defined water masses are labeled.

### 3.5 Diffusivity K

The vertical diffusivity, *K* was calculated from the advection-diffusion equation (equation 6) and can be seen in Figure 12. An approximately homogenous, very small *K* of 2 x $10^{-6}$ $m^2s^{-1}$ was calculated in the upper layers above the AW inflow. An apparent negative diffusivity was found in the lower layers, including the AW and IW. The bottom DW layer has weak diffusivity values of $10^{-7}$ $m^2s^{-1}$. Considering the homogeneity of the

top 7 layers and the non-physicality of a negative diffusivity, the average value of 2 x $10^{-6}$ $m^2s^{-1}$ was extended to the sea floor during following calculations.

The possible physical reasons for the apparent negative diffusivity in the lower section of the water column will be discussed in Section 4 below.

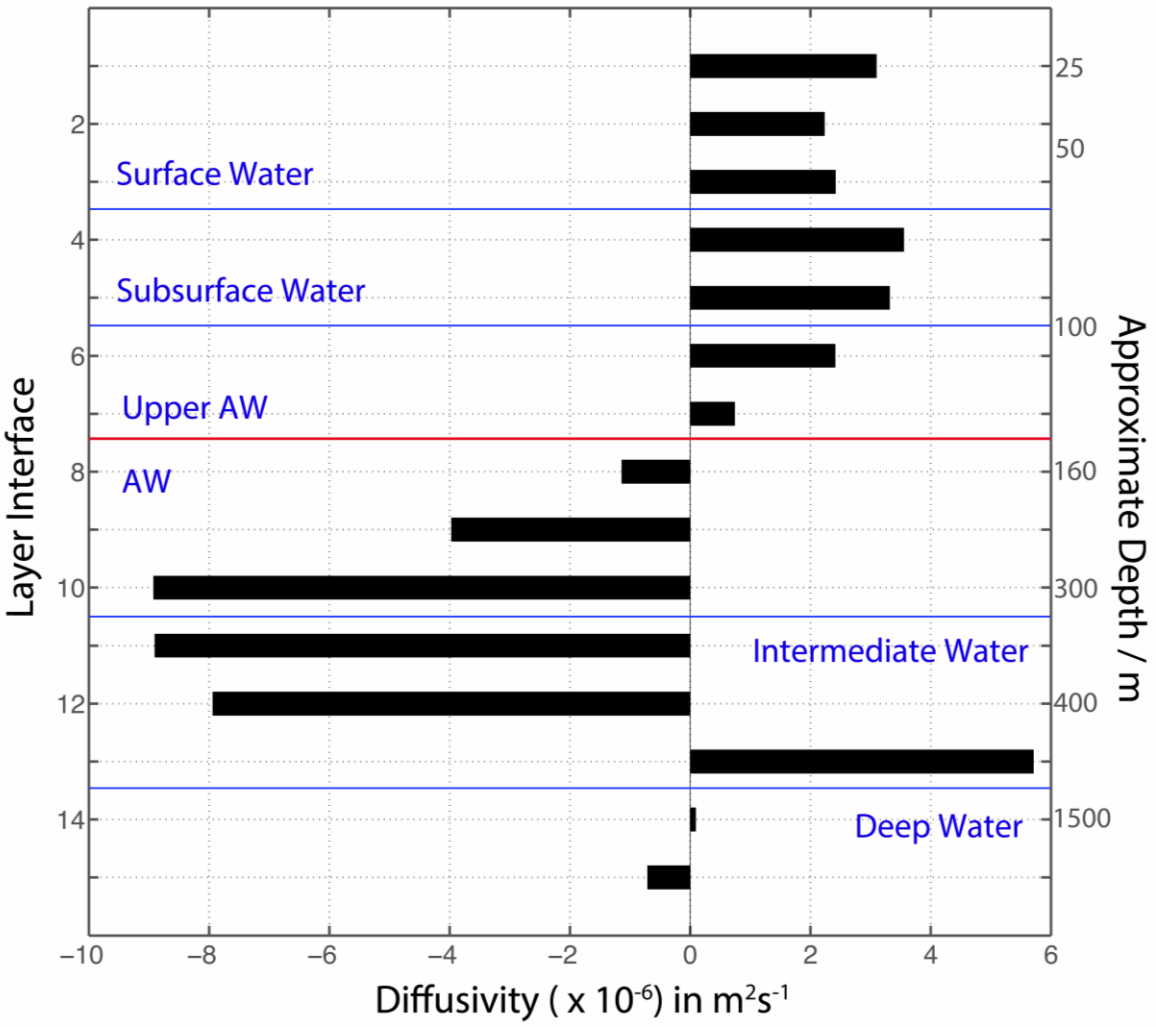


**Figure 12:** Graph of apparent diapycnal diffusivity *K* for each layer interface. The defined water masses are labeled. Red line indicates the change from positive to negative values.

### 3.6 Dissipation ϵ and Power P

The dissipation is calculated from equation 9. The average integrated value of $\epsilon$ across the depth and area of the Arctic was calculated as 9.90 x $10^{-10}$ W $kg^{-1}$ when measured using the calculated K for the first 7 layers of the model and a constant average $K$ of 2 x $10^{-6}$ $m^2s^{-1}$ for the deeper layers. The calculation was also made using a variable Γ (equation 10), and a smaller average value of 2.01 x $10^{-10}$ W $kg^{-1}$ was calculated for the whole water column. The power required to fuel this dissipation for the volume of the Arctic Ocean was calculated by integrating the dissipation by the area and depth of the ocean using equation 11. A value of 0.04 TW was calculated using a constant mixing efficiency, Γ, whilst a smaller power of 0.03 TW is required when using a variable Γ.

# 4. Discussion and Interpretation

In summary, the main results are a weak diapycnal mixing of ~2 x $10^{-6}$ $m^2s^{-1}$ in the upper layers of the Arctic up to ~200 m depth, and an apparent negative diffusivity in most of the underlying water column. This corresponds to an average dissipation rate of 2 x $10^{-10}$ $Wkg^{-1}$ which requires a power of 0.03 TW. The negative diffusivity makes it unlikely that the assumption that the system is in an approximate steady state and that all transformations in the Arctic are caused by mixing due to breaking of internal waves is true and shows that the dominant transformation process changes from the upper to the bottom layers.

The weak diapycnal diffusivity in the upper layers agrees with previous work (D'Asaro & Morison 1992, Zhang & Steele 2007, Lenn *et al.* 2009) and is likely caused by double diffusion, described in Section 1.2.3. Localized boundary mixing, possibly driven by tides, may be an important process to provide the energy required to mix the Arctic Ocean (Rippeth *et al.* 2015). The negative diffusivity in the lower layers is unphysical and the most likely mechanism driving it is the effects of the AW inflow causing internal mixing to become less dominant, specifically the buoyancy loss by down slope injection of dense shelf waters in the Barents Sea, which has been described in Section 1.2.4. The advection-diffusion model lacks surface fluxes, which transform water masses by adding or removing heat and/or freshwater. Other processes may also be affecting mixing in the Arctic Ocean.

## 4.1 Diapycnal Mixing in Upper Layers

### 4.1.1 Comparison with Microstructure Measurements

Recent Microstructure (MS) measurements from Rippeth *et al.* (2015) are compared with the results of this project in order to support these results. Rippeth *et al*. (2015) collected pan-Arctic MS measurements of turbulent kinetic energy dissipation using a loosely

tethered free-fall velocity microstructure profiler in the shelf break north of Svalbard, the area near Severnaya Zemlya and in the Canada Basin. These were collected from 2007 – 2013 for the upper 500 m of the water column. The average dissipation was found to be weak with substantially enhanced turbulent mixing over areas of sloping 3-D topography and it varied with depth (Figure 13).

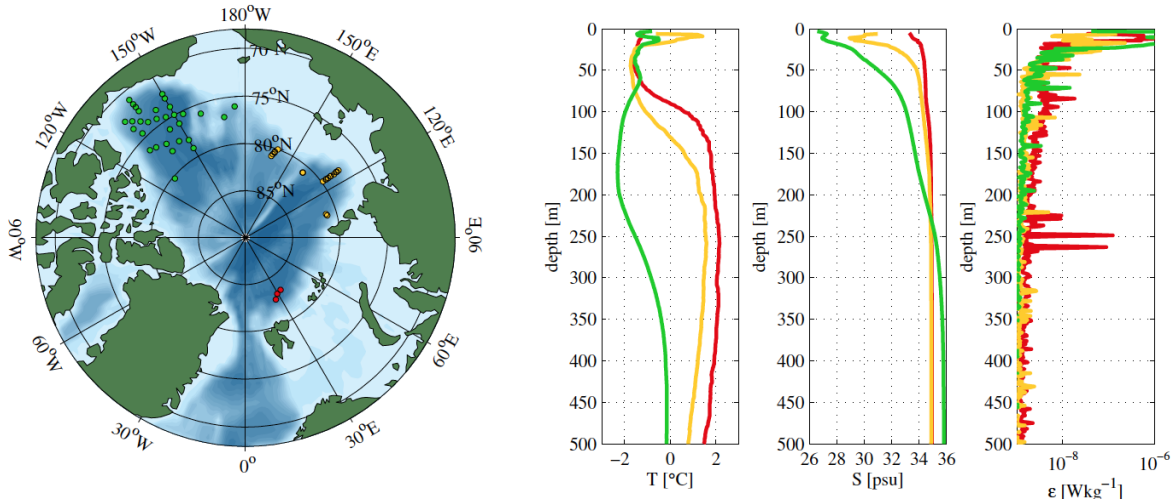


**Figure 13:** Map of the Arctic Ocean showing the location of the MS profiler measurements. The colours refer to the geographical location of the measurements. Mean temperature, salinity and dissipation profiles are shown for the three regions (green for Canada Basin, yellow for the area on continental shelf near Severnaya Zemlya, and red for region north of Svalbard) (Rippeth *et al.* 2015).

In the central Arctic where water depth is more than 2000 m, values of ~5 x $10^{-10}$ – 2 x $10^{-9}$ $Wkg^{-1}$ were observed, which are slightly larger than the values found here of 2 x $10^{-10}$ – 1 x $10^{-9}$ $Wkg^{-1}$ (Figure 14). This might indicate a source of mixing which was excluded during this project due to the assumptions used in the advection-diffusion equation, for example the effect of surface fluxes. These higher values may also be explained by the accuracy of the measurements. At depths of more than 500 m, approximately 95 % of the MS measurements were near or at the instrument noise level

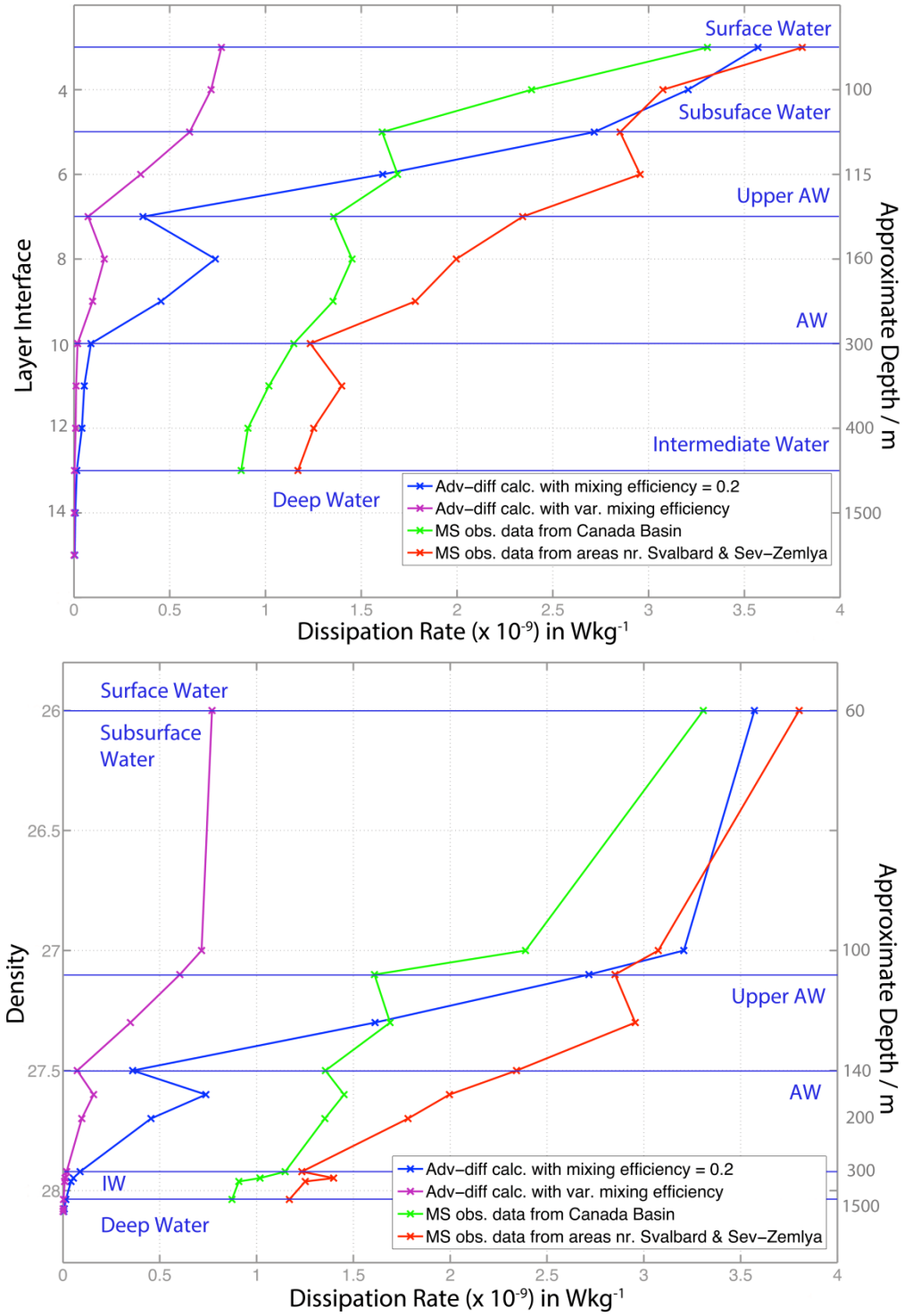


**Figure 14:** Dissipation Rate against (top) interfaces of the isopycnal layers and (bottom) density, for the results from advection-diffusion equation (blue using a constant mixing efficiency Γ of 0.2 and purple for a variable Γ) and MS observations (green for the deep ocean in Canada Basin and red for the mean of the areas on continental shelf).

(~$10^{-9}$ – $10^{-10}$ $Wkg^{-1}$, Lincoln, B. 2015, *pers. comm.*). This could make the MS dissipation value look higher than the real value when averaged out. These values compare with previously published figures such as Rainville & Winsor 2008, discussed in Section 1.2.3, which can be approximately converted to a dissipation value of ~1 x $10^{-10}$ $Wkg^{-1}$.

Over continental slope regions (water depth of 200 – 2000 m), the dissipation rate was measured as up to two orders of magnitude higher (Rippeth *et al.* 2015). The largest values were found to the north of Svalbard as 5 – 7 x $10^{-8}$ $Wkg^{-1}$. Previous work found mixing is enhanced near major topographic features, such as the Yermak plateau and its marginal seas (Padman & Dillon 1991; Sundfjord *et al.* 2007; Fer *et al.* 2010) and on bottom topography (D'Asaro & Morison 1992; Dewey *et al.* 1999) such as the Lomonosov ridge.

These results are illustrated and summarized in Figure 14, which compares the dissipation rate found using the advection diffusion equation both using a variable and a constant mixing efficiency, described in Section 2.4, with the MS measurements described above, separating the Canada Basin measurements with those taken near the boundaries. The lowest values are given by the advection-diffusion equation used here, whilst the MS measurements taken in the Canada basin are smaller than those measured at boundaries. In all cases there is a trend of decreasing dissipation rate with depth.

The power associated with the average MS dissipation (Rippeth *et al.* 2015) can be estimated as 0.25 TW. The power required to drive the dissipation using the values calculated during this project is 0.03 TW. Therefore, when considering both the results presented in Section 3.6 and the MS data as possible degrees of freedom, on average the power required to mix the Arctic is $0.03 \leq P \leq 0.25$ TW for the whole ocean and $0.01 \leq P \leq 0.03$ TW for the top 7 layers.

### 4.1.2 Sources of Dissipation

Weak tidal forces and the presence of sea ice have generally been used to explain the low energy levels of the Arctic Ocean. In this quiescent environment other mechanisms such as double diffusion, may be fundamental. This can be inferred from Figure 15 by DeLavergne *et al.* (2015), which shows a turbulent diffusivity model of the diapycnal diffusivity of heat and salt as a function of the turbulent intensity parameter, and the associated mixing regimes. In this context, the Arctic is in the buoyancy-controlled domain of turbulence where the regime becomes double-diffusive. Since double diffusion is driven by thermal molecular energy, it is very efficient, and the dissipation coefficient is small.

The MS measurements from Rippeth et al. (2015) show local variations of dissipation, with higher values near topography. These values are sufficiently large to drive significant turbulence and prevent thermohaline staircases from forming. Rippeth et al. (2015) plotted the longitudinal variation in dissipation calculated by MS measurements (Figure 16). This figure suggests that the energy supporting enhanced dissipation along continental slopes is tidal.

The energy needed to fuel dissipation may also originate from winds. In moored observations from the Chukchi Sea continental shelf in the western Arctic, Rainville & Woodgate (2009) found a strong seasonal signal in wind-driven vertical mixing that is correlated with the annual cycle of ice concentration. Declining sea ice cover may therefore increase mixing due to the increased momentum transfer from wind to ocean (Giles *et al*. 2012, Martin *et al.* 2014, Tsamados *et al.* 2014). However the MS measurements of Rippeth *et al.* (2015) in locations with varying sea ice conditions suggest that the dissipation in the intermediate and deep-water layers is not sensitive to sea ice conditions, and is caused by tides.

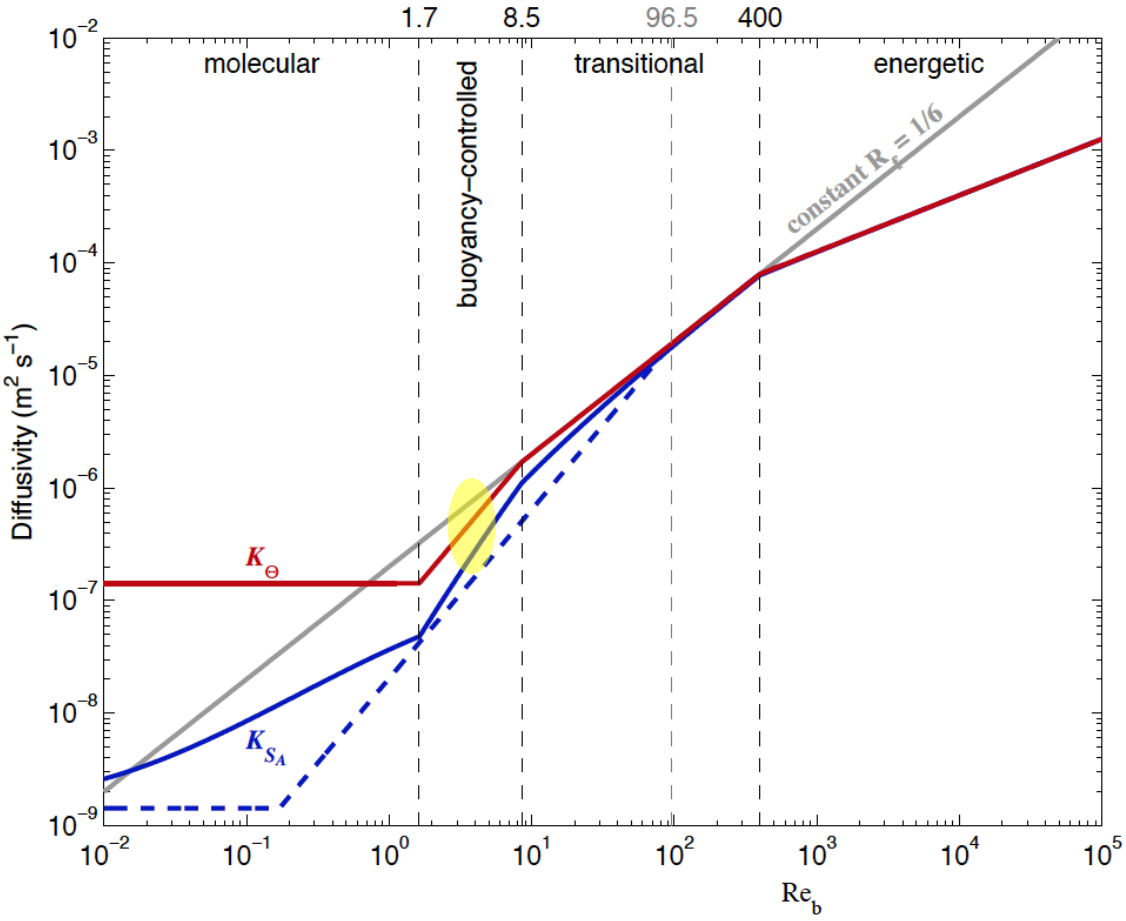


**Figure 15:** Turbulent diffusivity model based on Bouffard & Boegman (2013) and Jackson & Rehmann (2014) from DeLavergne *et al.* (2015). The diapycnal diffusivity ($m^2s^{-1}$) of (red) heat and (blue) salt as a function of the turbulent intensity parameter are shown. The dashed blue curve corresponds to the salt diffusivity parameterized by Bouffard & Boegman (2013) whereas the solid blue curve is deduced from the heat diffusivity (red) using the diffusivity ratio parameterization of Jackson & Rehmann (2014). Indicated regimes at the top only refer to the heat diffusivity. The thick grey line shows the diffusivities assuming a constant mixing efficiency of 0.17 ($\Gamma$ = 0.2). Yellow circle shows the area where the Arctic lies according to advection-diffusion calculation.

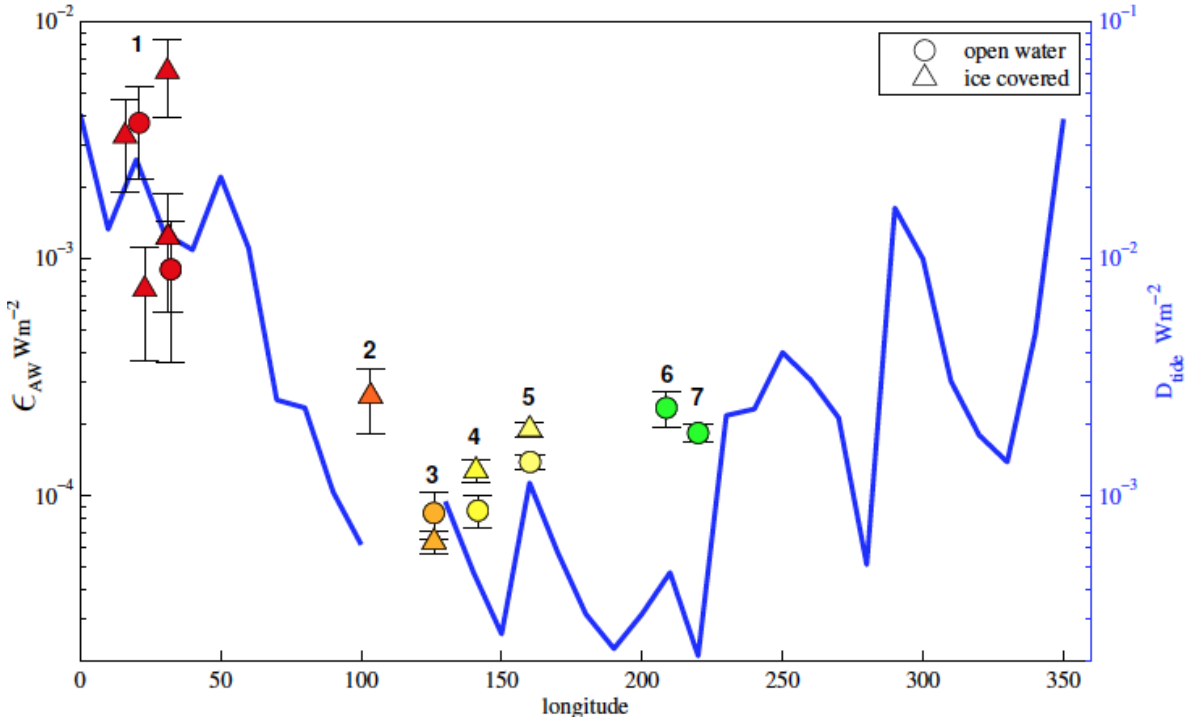


**Figure 16:** Transect mean AW dissipation across the AW thermocline plotted as a scatter plot against longitude. Blue line is the rate of tidal dissipation D computed as the difference between the work done by the tide generating force and the divergence of the tidal energy flux. (Rippeth *et al.* 2015).

### 4.1.3 A Conceptual Model for Mixing in the Arctic

What follows is an attempt at a simple conceptual model to reconcile the results of this project with the MS measurements. Whilst the results of this project are a basin-wide average with depth, the MS values suggest that the Arctic has different levels of mixing depending on location. The quiescent ocean basins have very small dissipation values and are thought to be double-diffusive. Areas with high slope have higher dissipation values and are thought to be powered by tides.

We start by assuming that the value for the power required to mix the Arctic Ocean calculated during this project of 0.03 TW is correct. This was inputted into Equation 11 in order to calculate the area that is required to be mixing in order to produce this value for

power, using various values for dissipation and keeping all other terms constant. This area was then converted into a percentage of the total Arctic Ocean surface area. A bathymetric map was used to estimate the slope (IBCAO) and calculate the percentage of the Arctic Ocean with bathymetric slope higher than certain values. These two figures were then compared (Figure 17).

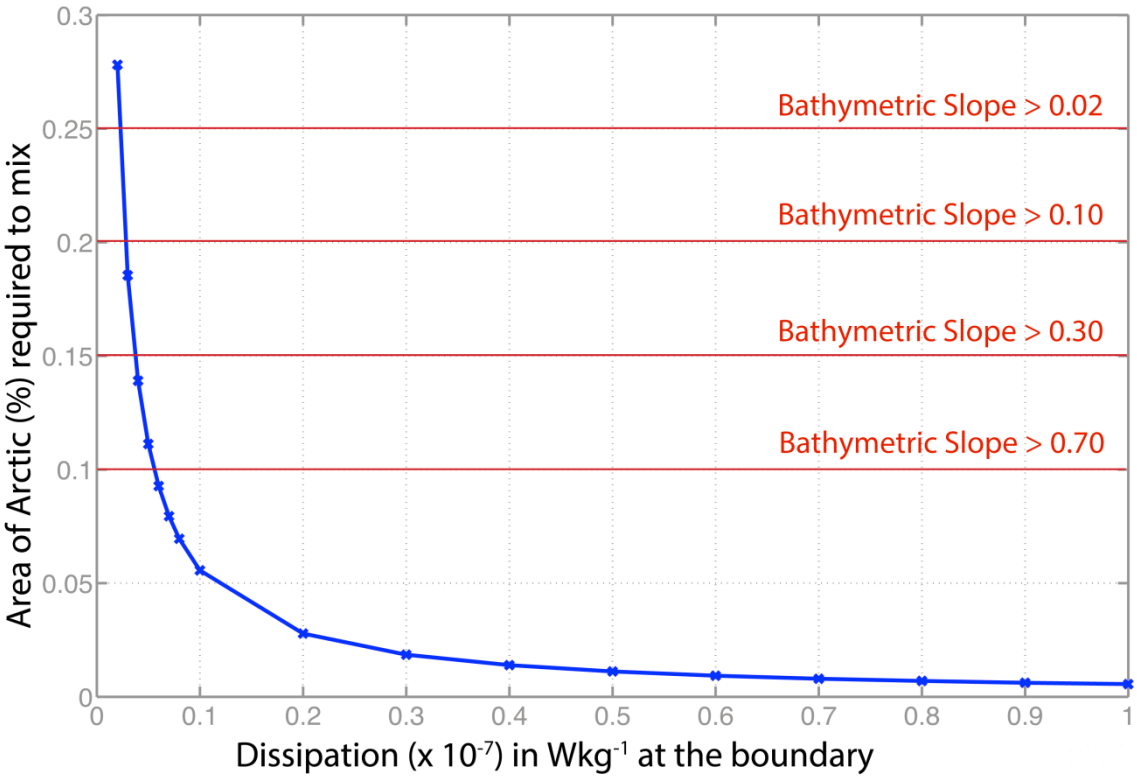


**Figure 17:** Plot of the percentage of area of the Arctic Ocean required to be mixing at varying rates of dissipation in order to provide the power required to mix this ocean calculated using the advection-diffusion equation. The bathymetric slope was also calculated and the percentage of the Arctic with a slope of more than certain values measured. These are shown in red.

If the Arctic was mixing at the higher dissipation values measured by the MS measurements at the Severnaya-Zemlya area, the area of the Arctic required to be actively mixing is 15%, which is the same percentage as areas with bathymetric slope of more than 0.30. This value is smaller than that produced by Fer *et al.* 2010, who estimated that the

areas near boundaries and over rough topography which can be assumed to be ‘hot spots’ of mixing make up 30 % of the Arctic Ocean surface area.

The areas with a bathymetric slope of more than 0.30 are plotted in Figure 18 (red shading). A step function is hypothesized with all mixing occurring in these locations and with double-diffusion taking place in the interior of the Arctic Ocean. Locations where there have been previously published observations of double-diffusion are also shown in Figure 18. There appears to be a correlation between areas of shallower bathymetric slope and the observations of double-diffusive fluxes, with few observed in the areas of high bathymetric slope.

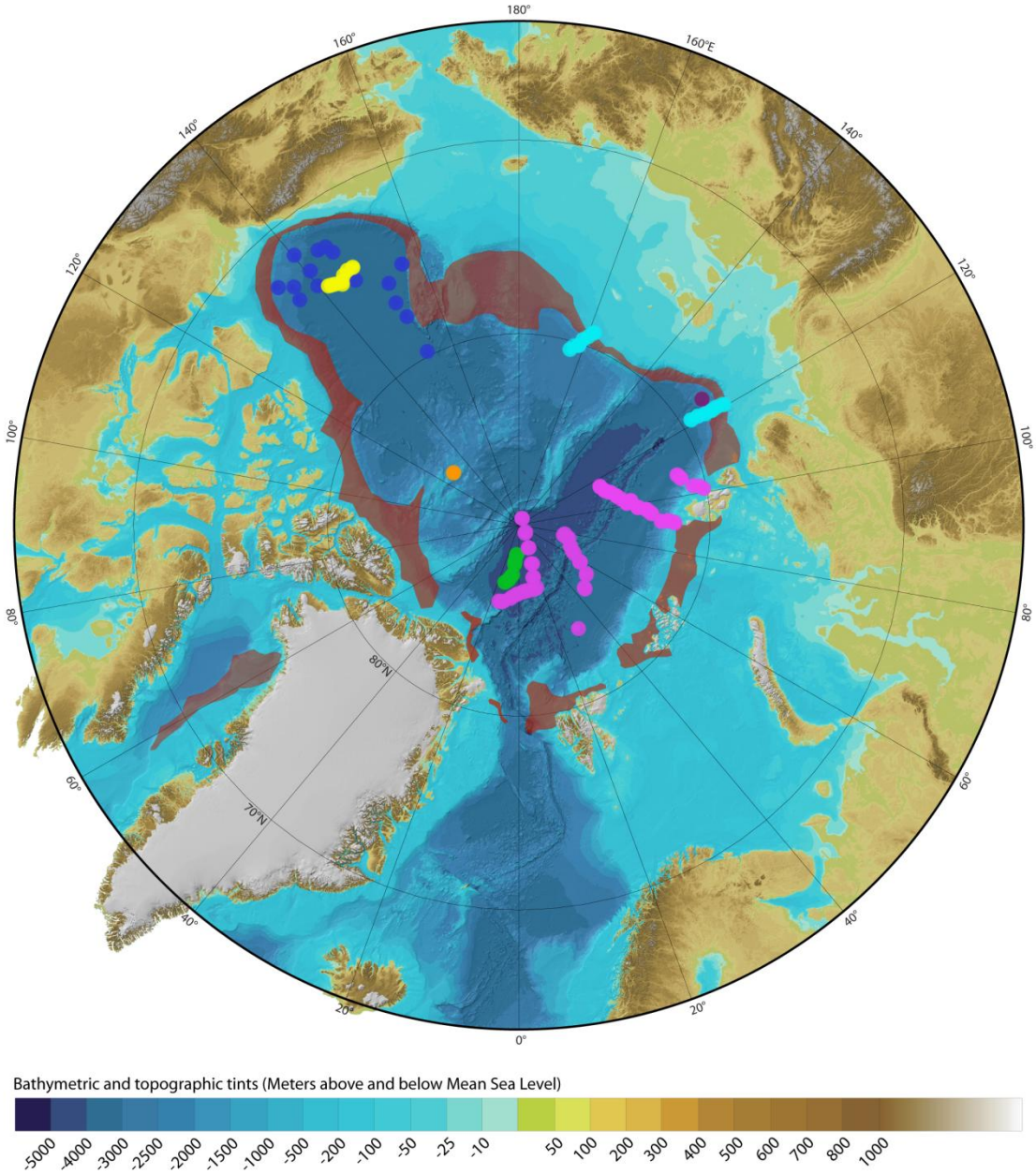


**Figure 18**: Bathymetric map of the Arctic (IBCAO) showing in red shading the areas where mixing is required in order to explain the background diffusivity measured by advection diffusion if the rate of mixing is equivalent to that measured by MS in the continental slope north of Svalbard, corresponding to places with a bathymetric slope of more than – 0.1. Dots correspond to places where double diffusive staircases have been observed, and are as follows: (orange) Neshyba *et al.* 1971, (yellow) Padman & Dillon 1987, (pink) Rudels *et al.* 1999, (blue) Timmermans *et al.* 2008, (cyan) Lenn *et al.* 2009, (purple) Polyakov *et al.* 2012, (green) Sirevaag & Fer 2012.

### 4.1.4 Heat Production in Background Mixing

The vertical heat flux due to diffusion has been calculated from:

$$F_H = \sigma_0 C_p K_z \frac{\delta T}{\delta z} \tag{12}$$

where $C_p$ is the ocean specific heat capacity and $F_H$ is positive upward. The calculated heat vertical flux for the UAW/AW interface is ~0.3 $Wm^{-2}$. This compares with those found by Lique *et al.* (2014) of $F_H$ ~ 0.1 - 0.3 $Wm^{-2}$ for the approximately equivalent depth range (~150 – 450 m depth). These weak heat fluxes are thought to be due to double diffusion. The major part of heat transfer in the Arctic is thought to occur along boundaries (Padman 1995), where the stratification of the upper ocean is weaker (Lenn *et al*. 2009).

Plots of the UAW/AW interface in March and September (Figure 19), created using the MIMOC dataset (Schmidtko *et al.* 2013), show that the largest Arctic heat loss is in the Barents Sea. This occurs because, unlike the rest of the Arctic Ocean, relatively large areas of the Barents Sea remain unfrozen, allowing large solar radiation during spring and summer and stronger heat loss in winter and autumn (Serreze *et al.* 2007). Thus, the inflowing AW into the Barents Sea becomes cooler and fresher, and dense water is formed (see Sections 1.2.4 & 1.2.5).

Figure 19 also suggests that there are large seasonal changes in the dynamics of the Arctic Ocean which might influence the results of this work. Since only summer data was used during the present project, the results of this work cannot be extended into an annual mean, but limited in showing the summer state of the Arctic Ocean.

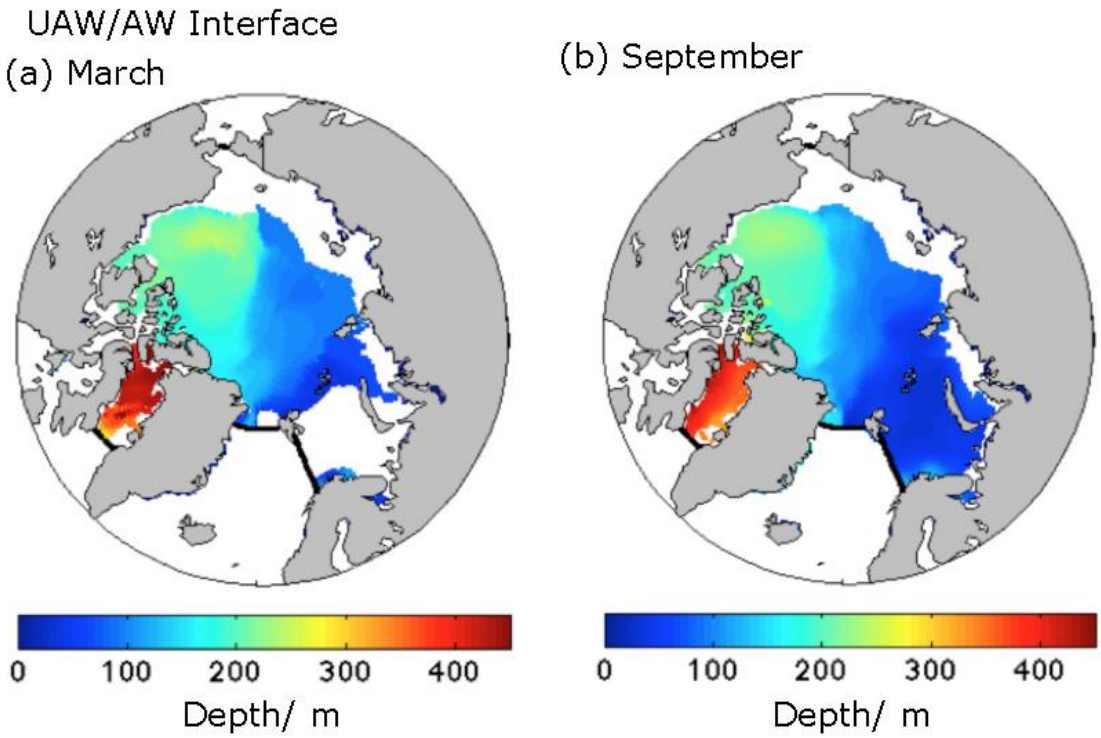


**Figure 19:** Plots of depth to UAW/AW interface and its distribution in (a) March and (b) September.

# 5. Conclusions and Future Work

Figure 20 is a schematic diagram showing a summary of the results discussed during this project. The main conclusion is that the Arctic Ocean has two different modes of water mass transformations. In the upper 400 m of the Arctic mixing is very weak (~ $10^{-6}$ $m^2s^{-1}$), as is consistent with observational measurements. This small number is thought to reflect previously observed double diffusive fluxes within the ocean basins away from topography. These are hypothesized to be ubiquitous in these regions. A small percentage of the ocean floor is believed to have tides which are strong enough to generate internal waves. The mechanical energy generated here might be enough to power dissipation for the whole Arctic Ocean. Whilst the value for diapycnal diffusivity is small compared to the estimated global average, this region represents only a small fraction of the global ocean area and therefore contributes little to the global integral.

An up-gradient buoyancy flux is necessary to maintain double-diffusive thermohaline staircases, therefore the diapycnal upwelling of AW requires additional processes in order to support it. These are likely to be caused by the large volume flux and heat input from the AW layer into the lower section of the water column of the Arctic. This is suggested from the larger volume fluxes and vertical velocities associated with the AW layer, with a vertical velocity of 1.4 x $10^{-7}$ $ms^{-1}$ towards the UAW and a similar value of -1.2 x $10^{-7}$ $ms^{-1}$ downwards towards the deeper layers. A down-welling cell is likely present in the mid to deep layers of the Arctic transforming some of the AW into denser deeper waters. This is possibly caused by the loss of buoyancy. Further work is required to analyze this.

The depth of the interface between these two different modes of mixing is related to the initial inflow of AW into the Arctic, where it sinks below the surface water due to its relatively high density. The deep waters of the Arctic are effectively isolated from the surface fluxes due to the weak vertical mixing. An average dissipation value for the whole

ocean column of 2 x $10^{-10}$ $Wkg^{-1}$ was calculated, which is similar to recent MS measurements (Rippeth *et al.* 2015). This corresponds to a required power of 0.03 TW to force mixing in the Arctic Ocean.

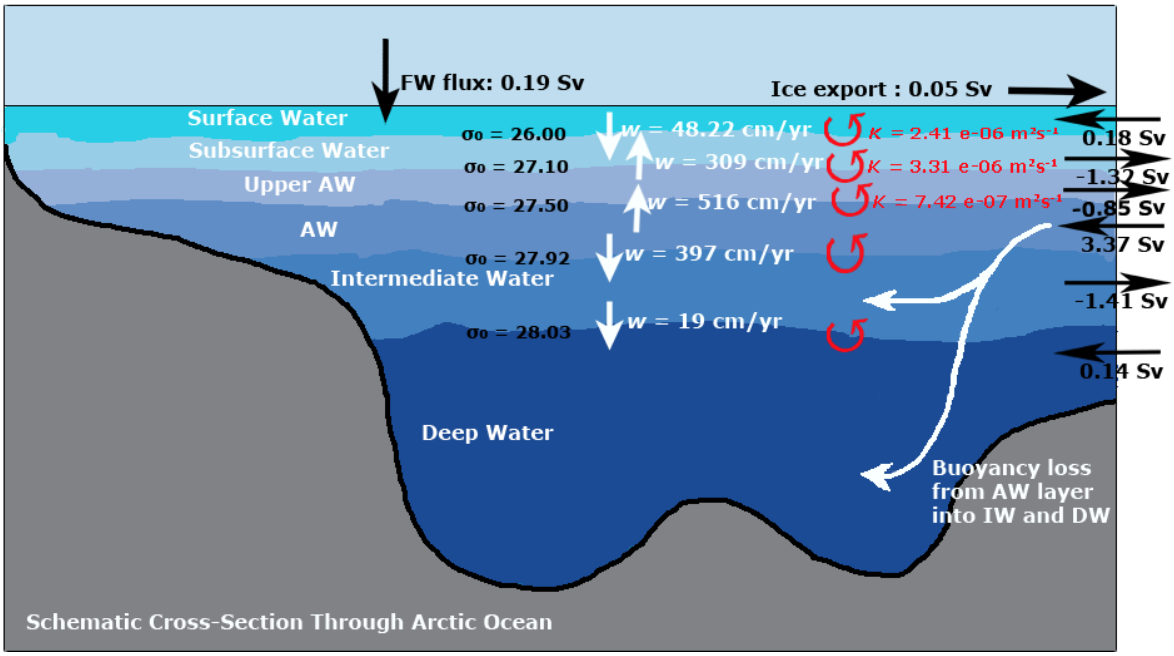


**Figure 20:** Schematic figure of the Arctic Ocean showing a summary of the results. The black arrows show the total flux through all the Arctic gateways into each water layer. The FW input from precipitation and river inflow, and the export of sea ice are also shown. The small white arrows show the vertical velocity, *w* across the water mass interfaces and the large white arrow signifies the injection of AW water into deeper layers. The red arrows show the turbulent eddy diffusivity *K*. The named water masses are labeled. Values for FW flux and ice export taken from Tsubouchi *et al.* 2012.

To further address the questions arising from and unconstrained by this project, thermohaline transformations of water masses could be estimated following the methods described in Evans *et al.* (2015). Here the diapycnal water mass transformations are estimated as fluxes across isotherms and isohalines in order to find the processes responsible for changes in the distribution of water masses in thermohaline coordinates. The water mass changes in thermohaline coordinates from the waters leaving the Arctic to

the water entering the Arctic can be calculated in order to find the path of least resistance in transforming the water masses inside the Arctic (Figure 21).

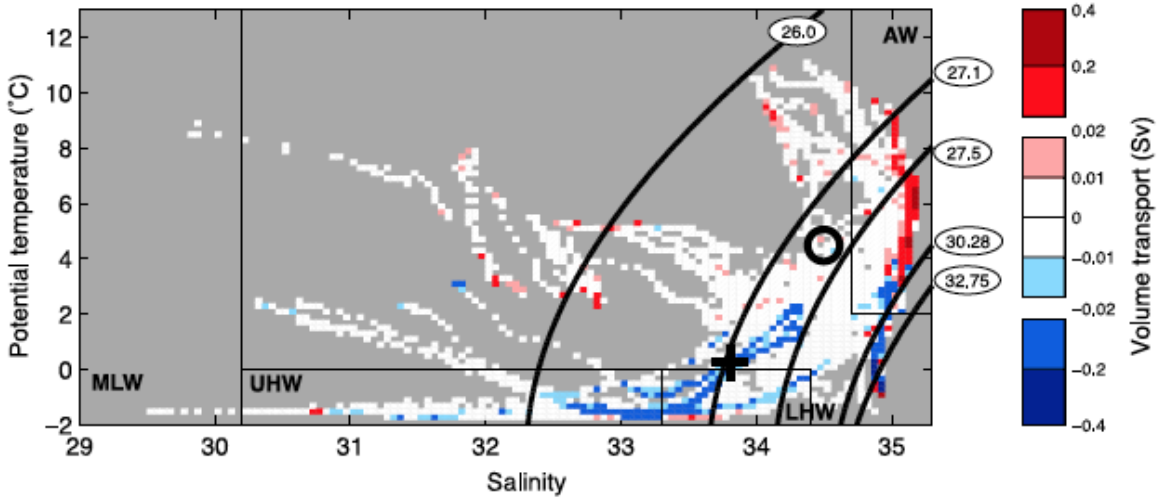


**Figure 21:** Volumetric $\theta$- S plot gridded with $\delta\theta$ = 0.2 $^{o}$C and $\delta$S = 0.05, Model water mass boundaries (densities) are shown in black. The corresponding densities are 26.0 $\sigma_0$, 27.1 $\sigma_0$, 27.5 $\sigma_0$, 30.28 $\sigma_{0.5}$ and 32.75 $\sigma_{1.0}$. Net transport per $\theta$-S grid box is shaded with red for inflow and blue for outflow (Sv). Grey shading indicates no data. The transport-weighted mean properties of the inflow (bold circle) are: salinity 34.50, potential temperature 4.49 $^{o}$C, density ($\sigma_0$) 27.34 kgm$^{-3}$; for the outflow (bold cross), including sea ice, they are 33.81, 0.25 $^{o}$C and 27.13 kg,$^{-3}$. Some conventional water masses in the central Arctic (MLW – Mixed Layer Water (SW), UHW – Upper Halocline Water (SW – SSW), LHW – Lower Halocline Water (SSW – UAW), and AW) are shown. Figure from Tsubouchi *et al.* 2012.

# 6. References


Aagaard, K., Swift, J. H. & Carmack, E. C. 1985. Thermohaline circulation in the Arctic Mediterranean seas, *Journal of Geophysical Research*, **90**, 4833-4846, doi:10.1029/JC090iC03p04833.

Aagaard, K. & Carmack, E. 1989. The role of sea ice and other fresh-water in the Arctic circulation. *Journal of Geophysical research*, **94** (C10), 14, 485 -14, 498, doi:10.1029/JC094iC10p14485.

Aagaard, K. & Roach, A. T. 1990. Arctic ocean-shelf exchange: Measurements in Barrow Canyon. *Journal of Geophysical Research*, **95**, doi:10.1029/90JC01139.

Aagaard, K. & Carmack, E. C. 1994. The Arctic Ocean and climate: A perspective, in *The Polar Oceans and Their Role in Shaping the Global Environment, Geophysical Monograph Series*, **85**, eds. Johannessen, O. M., Muench, R. D. & Overland, J. E, 5-20, AGU, Washington, D.C. doi:10.1029/GM085p0005.

Aksenov, Y., Ivanov, V. V., Nurser, A. J. G., Bacon, S., Polyakov, I. V., Coward, A. C., Naveira-Garabato, A. C. & Beszczynska-Möller, A. 2011. The Arctic Circumpolar Boundary Current. *Journal of Geophysical Research*, **116**, C9, doi:10.1029/2010JC006637.

Alford, M. H. 2010. Sustained, full-water-column observations of internal waves and mixing near Mendocino Escarpment. *Journal of Physical Oceanography*, **40**, 12, 2643-2660.

Antonov, J. I., Levitus, S., Boyer, T. P., Conkright, M. E., O'Brien, T. D. & Stephens C. 1998. *World Ocean Atlas 1998*, NOAA Atlas, U.S. Government Printing Office, Washington, DC.

Arneborg, L. 2002. Mixing efficiencies in patch turbulence. *Journal of Physical Oceanography*, **32**, 1496 – 1506.

Barnier, B., Madec, G., Penduff, T., Molines, J.-M., Treguier, A-M., Le Somme, J., Beckmann, A., Biastoch, A., Boning, C., Dengg, J., Derval, C., Durand, E., Gulev, S., Remy, E., Talandier, C., Theetten, S., Maltrud, M., McClean, J. & DeCuevas, B. 2006. Impact of partial steps and momentum advection schemes in a global ocean circulation model at eddy permitting resolution. *Ocean Dynamics*, **56**, 5-6, 543-567, doi:10.1007/s10236-006-0082-1.

Barry, M. E., Ivey, G. N., Winters, K. B. & Imbergr, J. 2001. Measurements of diapycnal diffusivities in stratified fluids. *Journal of Fluid Mechanics*, **442**, 59-291.

Beszczynska-Möller, A., Woodgate, R. A., Lee, C., Melling, H. & Karcher, M. 2011. A synthesis of exchanges through the main oceanic gateways to the Arctic Ocean. *Oceanography*, **24**, 3, 82-99, doi.10.5670/oceanog.2011.59.

Beszczynska-Möller, A., Fahrbach, E., Schauer, U. & Hansen, E. 2012. Variability in Atlantic water temperature and transport at the entrance to the Arctic Ocean, 1997 – 2010. *ICES Journal of Marine Science*, doi:10.1093/icesjms/fss056.

Bouffard, D. & Boegman, L. 2013. A diapycnal diffusivity model for stratified environmental flows. *Dynamics of Atmospheres and Oceans*, **61-62**, 13-43. Doi:10.1016/j.dynatmoce.2013.02.002.

Boyer, T. P., Levitus, S., Antonov, J. M., Conkright, M. E., O'Brien, T. & Stephens, C. 1998. *World Ocean Atlas 1998, Vol. 4, Salinity of the Atlantic Ocean*, NOAA Atlas NESDIS, **30**, 166, NOAA, Silver Spring, Md.

Broecker, W. S. 1991. The great ocean conveyor. *Oceanography*, **4**, 2, 79-89.

Carmack, E. C., Macdonald, R., Perkin, R., McLaughlin, F. & Pearson, R. 1995. Evidence for warming of Atlantic water in the southern Canadian Basin of the Arctic Ocean: Evidence from the Larsen-93 Expedition. *Geophysical Research letters*, **22**, 1061-1065.

Carmack, E. C., Aagaard, K., Swift, J. H., Macdonald, R. W., Mclaughlin, F. A., Jones, E. P., Perkin, R. G., Smith, J. N., Ellis, K. M. & Killius, L. R. 1997. Changes in temperature and tracer distributions within the Arctic Ocean: Results from the 1994 Arctic Ocean section. *Deep Sea Research, Part II*, **44**, 1487 – 1502, doi:10.1016/S0967-0645(97)00056-8.

Cuny, J., Rhines, P. B. & Kwok, R. 2005. Davis Strait volume, freshwater and heat fluxes. *Deep Sea Research, Part I*, **52**, (3), 519 – 542, doi:10.1016/j.dsr.2004.10.006.

Curry, B., Lee, C. M. & Petrie, B. 2011. Volume, freshwater, and heat fluxes through Davis Strait, 2004-05. *Journal of Physical Oceanography*, **41**, (3), 429 – 439, doi:10.1175/2010JPO4536.1.

D'Asaro, E. A. & Morison, J. H. 1992. Internal waves and mixing in the Arctic Ocean. *Deep Sea Research*, **39**, S459-S484.

De Lavergne, C., Madec, G., Le Somme, J., Nurser, A. J. G. & Naveira-Garabato, A. C. 2015. The impact of a variable mixing efficiency on the abyssal overturning circulation. *Journal of Physical Oceanography*, doi:10.1175/JPO-D-14-0259.1.

De Steur, L., Hansen, E., Gerdes, R., Karcher, M., Fahrbach, E. & Holfort, J. 2009. Freshwater fluxes in the East Greenland Current: A decade of observations. *Geophysical Research Letters*, **36**, L23611, doi:10.1029/2009GL041278.

Dewey, R., Muench, R. & Gunn, J. 1999. Mixing and vertical heat flux estimates in the Arctic Eurasian Basin. *Journal of Marine Systems*, **21**, 199-205.

Dmitrenko, I. A., Kirillow, S. A. & Tremblay, L.B. 2008. The long-term and interannual variability of summer fresh water storage over the eastern Siberian shelf: Implication for climatic change. *Journal of Geophysical Research*, **113,** C03007, doi:10.1029/2007JC004304.

Dmitrenko, I. A., Kirillov, S. A., Serra, N., Koldunov, N. V., Ivanov, V. V., Schauer, U., Polyakov, V., Barber, D., Janout, M., Lien, V. S., Makhotin, M. & Aksenov, Y. 2014. Heat Loss from the Atlantic water layer in the north Kara Sea: Causes and Consequences. *Ocean Science*, **10**, 719 – 730.

Environmental Working Group (EWG). 1997. *Joint U.S.-Russian Atlas of the Arctic Ocean for the Winter Period* (CD-ROM), National Snow and Ice Data Centre, Boulder, Colorado.

Environmental Working Group (EWG). 1998. Joint *U.S.-Russian Atlas of the Arctic Ocean for the Summer Period* (CD-ROM), National Snow and ice Data Centre, Boulder, Colorado.

Evans, D. G., Zika, J. D., Naveira-Garabato, A. C. & Nurser, A. J. G. 2015. The imprint of Southern Ocean overturning on seasonal water mass variability in Drake Passage. *Journal of Geophysical Research*, doi:10.1002/2014JC010097.

Fahrbach, E. & Lemke, P. 2005. The expedition ARKTIS-XXI/1 a and b of the Research Vessel "Polarstem" in 2005, in *ARK-XX/2 Cruise Report*, Eds. Budeus G., Fahrbach E. & Lemke, P. pp. 57 – 142, Germany.

Fer, I. 2009. Weak vertical diffusion allows maintenance of cold halocline in the central Arctic. *Atmospheric and Oceanic Science Letters*, **2**, 3, 148-152.

Fer, I., Skagseth, R. & Geyer, F. 2010. Internal waves and mixing in the marginal ice zone near the Yermak Plateau. *Journal of Physical Oceanography*, **40**, 1613-1630.

Ferrari, R. & Wunsch, C. 2009. Ocean Circulation Kinetic Energy: Reservoirs, Sources, and Sinks. *Annual Review of Fluid Mechanics*, **41**, 253-282, doi:10.1146/annurev.fluid.40.111406.102139.

Giles, K. A., Laxon, S. W., Ridout, A. L., Wingham, D. J. & Bacon, S. 2012. Western Arctic Ocean freshwater storage increased by wind-driven spin-up of the Beaufort Gyre. *Nature Geoscience*, **5**, 194-197. doi:10.1038/ngeo1379.

Grotefendt, K., Logemann, K., Quadfasel, D. & Ronski S. 1998. Is the Arctic Ocean warming? *Journal of Geophysical Research*, **103**, doi:10.1029/98JC02097.

Huussen, T. N., Naveira-Garabato, A. C., Bryden, H. L. & McDonagh, E. L. 2012. Is the deep Indian Ocean MOC sustained by breaking internal waves? *Journal of Geophysical Research*, **117**, C08024. doi:10.1029/2012JC008236.

IPCC. 2014. Climate Change 2014 *Synthesis Report. Contribution of Working Groups I, II and III to the Fifth Assessment Report of the Intergovernmental Panel on Climate Change*. IPCC, Geneva, Switzerland.

Jackson, J. M., Williams, W. J. & Carmack, E. C. 2012. Winter sea-ice melt in the Canada Basin, Arctic Ocean. *Geophysical Research Letters*, **39**, L03603, doi:10.1029/2011GL050219.

Jackson, P. M. & Rehmann, C. R. 2014. Experiments on differential scalar mixing in turbulence in a sheared, stratified flow. *Journal of Physical Oceanography*, **44**, 2661-2680. doi:10.1175/JPO-D-14-0027.1.

Jeffries, M. O., Richter-Menge, J. A. & Overland, J. E. 2013. Arctic Report Card 2013.
http://www.arctic.noaa.gov/reportcard. *Accessed November 2014*.

Kagan, B. A., Sofina, E. V. & Timofeev, A. A. 2010. On Diapycnal Mixing Induced by Internal Tidal Waves in the Arctic Ocean. *Atmospheric and Oceanic Physics*, **46**, 2, 224-231.

Karcher, M. J., Gerdes, R., Kauker, F. & Koberle, C. 2003. Arctic warming: Evolution and spreading of the 1990s warm event in the Nordic seas and the Arctic Ocean. *Journal of Geophysical Research*, **108**, 3034, doi:10.1029/2001JC001265.

Kelley, D. E., Fernando, H. J. S., Gargett, A. E., Tanny, J. & Özsoy, E. 2003. The diffusive regime of double diffusive convection. *Progressive Oceanography*, **56**, 461-481. Doi:10.1016/S0079-6611(03)00026-0.

Kowalik, A. & Proshutinsky, A. Y. 1993. The diurnal tides in the Arctic Ocean. *Journal of Geophysical Research*, **98**, 16, 449-468.

Kowalik, A. Y. & Kowalik, Z. 1995. Topographic enhancement of tidal motion in the western Barents Sea. *Journal of Geophysical Research*, **100**, C2, 2613-2637.

Kwok, R. 2009. Outflow of Arctic Ocean sea ice into the Greenland and Barents Seas: 1979 – 2007. *Journal of Climate*, **22**, 2, 438-2, doi.10.1175/2008JCLI2819.1.

Large, W. G., McWilliams, J. C. & Doney, S. C. 1994. Oceanic Vertical Mixing: A review and a model with a nonlocal boundary-layer parameterization. *Review of Geophysics*, **32**, 4, 363-403, doi:10.1029/94RG01872.

Ledwell, J. R., Montgomery, E. T., Polzin, K. L., St. Laurent, L. C., Schmitt, R. W. & Toole, J. M. 2000. Evidence for enhanced mixing over rough topography in the abyssal ocean. *Nature*, **403**, 182-189.

Lee, C. M., Abriel, J., Gabat, J. I., Petrie, B., Scotney, M., Soukhovtsev, V. & Thiel, K. V. 2004. An observational array for high-resolution, year-round measurements of volume, freshwater and ice flux variability in Davis Strait: *Cruise report for R/V Knorr 179-05, 22 September – 4 October 2004*, Univ. of Wash. Seattle, Wash. [Available at http://iop.apl.washington .edu/projects/ds/html/publications.php/APL_UW_TR_0408.pdf.]

Lenn, Y. D., Wiles, P. J., Torres-Valdes, S., Abrahamsen, E. P., Rippeth, T. P., Simpson, J. H., Bacon, S., Laxon, S. W., Polyakov, I., Ivanov, V. & Kirillov, S. 2009. Vertical mixing at intermediate depths in the Arctic boundary current. *Geophysical Research Letters*, **36**, L05601, doi:10.1029/2008GL036792.

Lenn, Y. D., Rippeth, T. P., Old, C. P., Bacon, S., Polyakov, I., Ivanov, V. & Hölemann, J. 2011. Intermittent Intense Turbulent Mixing under Ice in the Laptev Sea Continental Shelf. *Journal of Physical Oceanography*, **41**, 531-547.

Levine, M. D., Paulson, C. A. & Morison, J. H. 1985. Internal waves in the Arctic Ocean: Comparison with lower latitude observations. *Journal of Physical Oceanography*, **15**, 6, 800-809.

Lique, C. & Steele, M. 2013. Seasonal to decadal variability of Arctic Ocean heat content: A model-based analysis and implications for autonomous observing systems. *Journal of Geophysical Research*, **118**, 4, 1673-1695.

Lique C., Guthrie, J. D., Steele, M., Proshutinsky, A., Morison, J. H. & Krishfield, R. 2014. Diffusive vertical heat flux in the Canada Basin of the Arctic Ocean inferred from moored instruments. *Journal of Geophysical Research, Ocean*, **119**, 496-508. doi:10.1002/2013JC009346.

Lumpkin, R. & Speer, K. 2003. Large-scale vertical and horizontal circulation in the North Atlantic Ocean. *Journal of Physical Oceanography*, **33**, 1902-1920.

Manabe, S. & Stouffer, R. J. 1994. Multiple-Century Response of a Coupled Ocean-Atmosphere Model to an Increase of Atmospheric Carbon Dioxide. *Journal of Climate*, **7**, 5-23.

Martin, S. & Cavalieri, D. L. 1989. Contributions of the Siberian Shelf polynyas to the Arctic Ocean Intermediate and Deep Water. *Journal of Geophysical Research*, **94**, 12727-12738.

Martin, T., Steele, M. & Zhang, J. 2014. Seasonality and long-term trend of Arctic Ocean surface stress in a model. *Journal of Geophysical Research: Oceans*, **119** (3), 1723-1738. doi:10.1002/2013JC009425.

Mauritzen, C. 1996. Production of dense overflow waters feeding the North Atlantic across the Greenland-Scotland Ridge. Part 1: Evidence for a revised circulation scheme. *Deep Sea Research, Part I*, **43**, 769-806.

May, B. D. & Kelley, D. E. 2001. Growth and steady-state stages of thermohaline intrusions in the Arctic Ocean. *Journal of Geophysical Research*, 16783 – 16794.

McLaughin, F. A., Carmack, E.C., Williams, W. J., Zimmermann, S., Shimada, K. & Itoh, M. 2009. Joint effects of boundary currents and thermohaline intrusions on the warming of Atlantic water in the Canada Basin, 1993 – 2007. *Journal of Geophysical Research*, **114**, C00A12. Doi:10.1029/2008JC005001.

McPhee, M. G., Proshutinsky, A., Morison, J. H., Steele, M. & Alkire, M. B. 2009. Rapid change in freshwater content of the Arctic Ocean. *Geophysical Research Letters*, **36**, L10602, doi:10.1029/2009GL037525.

Melling, H., Lake, R. A., Topham, D. & Fissel, D. 1984. Oceanic thermal structure in the western Canadian Arctic. *Continental Shelf Research*, **3**, 223-258.

Merrifield, M. & Pinkel, R.1996. Inertial currents in the Beaufort Sea: Observations of response to wind and shear. *Journal of Geophysical Research*, **101**, 6577 – 6590.

Morison, J. H., Steele, M. & Andersen, R. 1998. Hydrography of the upper Arctic Ocean measured from nuclear submarine USS Pargo. *Deep Sea Research I*, **45**, 15-35.

Munk, W. 1966. Abyssal Recipes. *Deep-Sea Research*, **13**, 707-730.

Munk, W. & Wunsch, C. 1998. Abyssal recipes II: energetics of tidal and wind mixing. *Deep-Sea Research I*, **45**, 1977-2010.

Neshyba, S., Neal, V. T. & Denner, W. 1971. Temperature and conductivity measurements under ice island T-3. *Journal of Geophysical Research*, **76**, (33), 8107-8120. doi:10.1029/JC076i033p08107.

Osborn, T. R. 1980. Estimates of the local rate of vertical diffusion from dissipation measurements. *Journal of Physical Oceanography*, **10**, 89-89.

Östlund, H. G., Craig, H. C., Broecker, W. S. & Derek, W. 1987. GEOSECS Atlantic, Pacific and Indian Ocean Expeditions: Shorebased Data and Graphics. *National Science Foundation, US Government Printing Office, Washington, D. C.* **7,** 200 pp.

Padman, L. 1995. Small-scale physical processes in the Arctic Ocean. *In:* Arctic Oceanography: Marginal Ice Zones and Continental Shelves, Coastal and Estuarine Studies, 49. *Eds*: Smith, W. O. & Grebmeier, J. M., pp. 97–129.

Padman, L. & Dillon, T. M. 1987. Vertical heat fluxes through the Beaufort Sea thermohaline staircase. *Journal of Geophysical Research*, **92**, 10799-10806.

Padman, L. & Dillon, T. M. 1988. On the horizontal extent of the Canada Basin thermohaline steps. *Journal of Physical Oceanography*, **18**, 1458-1462.

Padman, L. & Dillon, T. M. 1991. Turbulent mixing near the Yermak Plateau during the Coordinated Eastern Arctic Experiment. *Journal of Geophysical Research*, **96**: doiL10.1029/90JC02260.

Padman, L., Plueddemann, A. J., Muench, R. D. & Pinkel, R. 1992. Diurnal tides near the Yermak Plateau. *Journal of Geophysical Research*, **97**. doi:10.1029/92JC01097.

Padman, L. & Erofeeva, S. 2004. A barotropic inverse tidal model for the Arctic Ocean. *Geophysical Research Letters*, **31** (2), doi:10.1029/2003GL019003.

Peltier, W. R. & Caulfield, C. P. 2003. Mixing Efficiency in Stratified Shear Flows. *Annual Reviews of Fluid Mechanics*, **35**, 135-167.

Pickart, R. S., Torres, D. J. & Clarke, R. A. 2002. Hydrography of the Labrador Sea during active convection. *Journal of Physical Oceanography*, **32**, 428-457.

Pickart, R. S., Spall, M. A., Ribergaard, M. H., Moore, W. K. & Milliff, R. F. 2003. Deep convection in the Irminger Sea forced by the Greenland tip jet. *Nature*, **424**, 152-156.

Plueddemann, A. J., Krishfield, R., Takizawa, T., Hatekeyama, K. & Honjo, S. 1998. Upper ocean velocities in the Beaufort Gyre. *Geophysical Research Letters*, **25**, 183-186.

Polyakov, I. V., Alekseev, G. V., Timokhov, L. A., Bhatt, U. S., Colony, R. L., Simmons, H. L., Walsh, D., Walsh, J. E. & Zakharov, V. F. 2004. Variability of the Intermediate Atlantic Water of the Arctic ocean over the Last 100 Years. *Journal of Climate*, **17**, 4485-4497, doi:10.1175/JCLI-3224.1.

Polyakov, I. V., Beszczynska, A., Carmack, E. C., Dmitrenko, I. A., Fahrbach, E., Frolov, I. E., Gerdes, R., Hansen, E., Holfort, J., Ivanov, V. V. *et al*. 2005. One more step toward a warmer Arctic. *Geophysical Research Letters*, **32**, L17605, doi:10.1029/2005GL023740.

Polyakov, I. V., Alexeev, V. A., Belchansky, G. I., Dmitrenko, I. A., Ivanov, V. V., Kirillov, S. A., Korablev, A. A., Steele, M., Timokhov, L. A. & Yashayaev, I. 2008. Arctic Ocean freshwater changes over the past 100 years and their causes. *Journal of Climate*, **21**, 364-384,doi:10.1175/2007JCLI1748.1.

Polyakov, I. V., Alexeev, V. A., Ashik, I. M., Bacon, S., Beszczynska-Möller, A., Carmack, E. C., Dmitrenko, I. A., Fortier, L., Gascard, J.-C., Hansen, E., Hölemann, E., Ivanov, V. V., Kikuchi, T., Kirillov, S., Lenn, Y.-D. McLaughlin, F. A., Piechura, J., Repina, I., Timokhov, L. A., Walczowski, W. & Woodgate, R. 2011. Fate of Early 2000s Arctic Warm Water Pulse. *Bulletin of American Meteorological Society*, **92**, 561-566.

Polyakov, I. V., Walsh, J. E. & Kwok, R. 2012. Recent Changes of Arctic Multiyear Sea Ice Coverage and the Likely Causes. *Bulletin of the American Meteorological Society*, **93**, 145-151.

Polzin, K. L., Toole, J. M. & Schmitt, R. W. 1995. Finescale parameterizations of turbulent dissipation. *Journal of Physical Oceanography*, **25**, 306-328.

Ponomarev, V. I. & Fel'zenbaum, A. I. 1975. 2-D non-stationary model of wind driven circulation in the Arctic Basin. *Okealogia XV*, **6**, 17-23.

Proshutinsky, A. Y. 1988. Modelling seasonal fluctuations of the level of the Arctic Ocean. *Soviet Meteorology and Hydrology*, **2**, 57-65.

Proshutinsky, A. Y. 1993. *The Arctic Ocean Level Oscillations*. Gidrometeoizdat, St. Petersburg, Russia.

Proshutinsky, A., Krishfield, R., Timmermans, M.-L., Toole, J., Carmack, E., McLaughlin, F., Zimmerman, S., Itoh, M. & Shimada, K. 2009. Beaufort Gyre freshwater reservoir: State and variability from observations. *Journal of Geophysical Research*, **114**, C1, doi:10.1029/2008JC005104.

Quadfasel, D., Frische, A. & Cresswell, G. 1996. The circulation in the source area of the South Equatorial Current in the eastern Indian Ocean. *Journal of Geophysical Research*, **101**, doi:10.1029/96JC00437.

Rabe, B., Schauer, U., Mackensen, A., Karcher, M., Hansen, E. & Beszczynksa-Möller. 2009. Freshwater components and transports in the Fram Strait – recent observations and changes since the late 1990s. *Ocean Science*, **5**, (3), 219-233, doi:10.5194/os-5-219-2009.

Rainville, L. & Winsor, P. 2008. Mixing across the Arctic Ocean: Microstructure observations during the Beringia 2005 Expedition. *Geophysical Research Letters*, **35**, L08606, doi:10.1029/2008GL033532.

Rainville, L. & Woodgate, R. A. 2009. Observations of internal wave generation in the seasonally ice-free Arctic. *Geophysical Research Letters*, **36**, L23604, doi:10.1029/2009GL041291.

Rehmann, C. R. & Koseff, J. R. 2004. Mean potential energy change in stratified grid turbulence. *Dynamics of Atmosphere and Oceans*, **37**, 271-294: doi:10.1016/j.dynatmocel.2003.09.001.

Rigor, I. G., Colony, R. L. & Martin, S. 2000. Variations in Surface Air Temperature Observations in the Arctic, 1979-97. *Journal of Climate*, **13**, 896-914.

Rippeth, T. P., Lincoln, B. L., Lenn, Y.-D., Green, J. A. M., Sundfjord, A. & Bacon, S. 2015. Tide-mediated warming of Arctic halocline by Atlantic heat fluxes over rough topography. *Nature Geoscience*, **8**, 191-194.

Roach, A., Aagaard, K., Pease, C., Salo, S., Weingartner, T., Pavlov, V. & Kulakov, M. 1995. Direct measurements of transport and water properties through the Bering Strait. *Journal of Geophysical Research*, **100**, C9, 18, 443-18, doi:10.1029/95JC01673.

Ronski, S. & Budeus, G. 2005. Time series of winter convection in the Greenland Sea. *Journal of Geophysical Research*, **110**, C4, doi:10.1029/2004JC002318.

Rudels, B. 1986. The outflow of polar water through the Arctic Archipelago and the oceanographic conditions in Baffin Bay. *Polar Research*, **4**, 161-180, doi:10.111/j.1751-8369.1986.tb00528.x.

Rudels, B., Jones, E. P., Anderson, L. G. & Kattner, G. 1994. On the intermediate depth waters of the Arctic Ocean, In: *The Polar Oceans and Their Role in Shaping the Global Environment: The Nansen Centennial Volume*, *Geophysical Monograph Series*, **85**, Eds. Johannessen, O. M., Muench, R. D. & Overland, J. E. 33-46, AGU, Washington, D.C.

Rudels, B., Bjork, G., Muench, R. D. & Schauer, U. 1999. Double-diffusive layering in the Eurasian Basin of the Arctic Ocean. *Journal of Marine Systems*, **21**, 3-27.

Rudels, B., Mamela, M. & Eriksson, P. 2008. Constraints on estimating mass, heat and freshwater transports in the Arctic Ocean: An exercise, In: *Arctic-Subarctic Ocean Fluxes: Defining the Role of the Northern Seas in Climate*, Eds. Dickson, R. R., Meincke, J. & Rhines, P. pp. 315-341, Springer, Dordrecht, Netherlands.

Schauer, U., Loeng, H., Rudels, B., Ozhigin, V. K. & Dieck, W. 2002. Atlantic Water flow through the Barents and Kara Seas. *Deep Sea Research, Part I*, **49**, (12), 2281-2298, doi:10.1016/S0967-0637(02)00125-5.

Schauer, U., Beszczynska-Möller, A. Walczowski, W., Fahrbach, E., Piechura, J. & Hansen, E. 2008. Variation of measured heat flow through the Fram Strait between 1997 and 2006, In: *Arctic-Subarctic Ocean Fluxes: Defining the Role of the Northern Seas in Climate*, Eds. Dickson, R. R., Meincke, J. & Rhines, P. pp. 65-85, Springer, Dordrecht, Netherlands.

Schauer, U. & Beszczynska-Möller, A. 2009. Problems with estimation and interpretation of oceanic heat transport – Conceptual remarks for the case of Fram Strait in the Arctic Ocean. *Ocean Sciences*, **5**, (4), 487-494, doi:10.5194/os-5-487-2009.

Schmidtko, S., Johnson, G. C. & Lyman, J. M. 2013. MIMOC: A Global Monthly Isopycnal Upper-Ocean Climatology with Mixed Layers. *Journal of Geophysical Research – Oceans*, **118**, 4, 1658-1672.

Serreze, M. C., Holland, M. M. & Stroeve, J. 2007. Perspectives on the Arctic's Shrinking Sea-Ice Cover. *Science*, **315**, 1533, doi:10.1126/science.1139426.

Serreze, M. C., Barrett, A. P., Stroeve, J. C., Kindig, D. N. & Holland, M. M. 2009. The emergence of surface-based Arctic amplification. *The Cryosphere*, **3**, 11-19.

Shapiro, G. I., Huthnance, J. M. & Ivanov, V. V. 2003. Dense water cascading off the continental shelf. *Journal of Geophysical Research: Oceans*, **108**, C12, 3390.

Shih, L. H., Koseff, J. R., Ivey, G. N. & Ferziger, J. H. 2005. Parameterization of turbulent fluxes and scales using homogenous sheared stably stratified turbulence simulations. *Journal of Fluid Mechanics*, **525**, 193-214.

Shiklomanov, A. I. & Lammers, R. B. 2009. Record Russian river discharge in 2007 and the limits of analysis. *Environmental Research Letters*, **4**, 045015, doi:10.1088/1748-9326/4/4/045015.

Simmons, H. L., Hallberg, R. W. & Arbic, B. K. 2004. Internal wave generation in a global baroclinic tide model. *Deep Sea Research, Part II*, **51**, 3043-3068.

Sirevaag, A. & Fer, I. 2012. Vertical heat transfer in the Arctic Ocean: The role of double-diffusive mixing. *Journal of Geophysical Research: Oceans*, **117**, C7, doi:10.1029/2012JC007910.

Skagseth, O., Furevik, T., Ingvaldsen, R. B., Loeng, H., Mork, K. A., Orvik, K. A. & Ozhigin, V. 2008. Volume and heat transports to the Arctic Ocean via the Norwegian and Barents seas, In: *Arctic-Subarctic Ocean Fluxes: Defining the Role of the Northern Seas in Climate*, Eds: Dickson, R. R., Meincke, J. & Rhines, P. pp. 45-64, Springer, Dordrecht, Netherlands.

Smedsrud, L. H., Ingvaldsen, R., Nilsen, J. E. O. & Skagseth, O. 2010. Heat in the Barents Sea: Transport, storage and surface fluxes. *Ocean Sciences*, **6**, (1), 219-234, doi:10.5194/os-6-219-2010.

Spielhagen, R. F., Werner, K., Sorensen, S. A., Zamelczyk, K., Kandiano, E., Budeus, G., Husum, K., Marchitto, T. M. & Hald, M. 2011. Enhanced Modern Heat Transfer to the Arctic by Warm Atlantic Water. *Science*, **331**, 6106, 450-453.

Steele, M., Morley, R. & Ermold, W. 2001. PHC: A global ocean hydrography with a high quality Arctic Ocean. *Journal of Climate*, **14**, 2079-2087, doi:10.1175/1520-0442(2001)014<2079:PAGOHW>2.0.CO.2.

Steele, M., Zhang, J. & Ermold, W. 2010. Mechanisms of summertime upper Arctic Ocean warming and the effect on sea ice melt. *Journal of Geophysical Research*, **115**, C11004. doi:10.1029/2009JC005849.

Steele, M., Ermold. W. & Zhang, J. 2011. Modeling the formation and fate of the near-surface temperature maximum in the Canadian Basin of the Arctic Ocean. *Journal of Geophysical Research*, **116**, C15, C11015, doi:10.1029/2010JC006803.

Stigebrandt, A. & Aure, J. 1989. Vertical Mixing in Basin Waters of Fjords. *Journal of Physical Oceanography*, **19**, 7, 917-926.

Sundfjord, A., Fer, I., Kasajima, Y. & Svendsen, H. 2007. Observations of turbulent mixing and hydrography in the marginal ice zone of the Barents Sea. *Journal of Geophysical Research: Oceans*, **112**, C5: doi:10.1029/2006JC003524

Timmermans, M.-L. & Garrett, C. 2006. Evolution of the Deep Water in the Canadian Basin in the Arctic Ocean. *Journal of Physical Oceanography*, **36**, 866-874: doi.10.1175/JPO2906.1.

Timmermans, M.-L., Toole, J., Krishfield, R. & Winsor, P. 2008. Ice-Tethered Profiler observations of the double-diffusive staircase in the Canada Basin thermocline. *Journal of Geophysical Research*, **113**, C00A02, doi.10.1175/2007JPO3782.1.

Toole, J. M., Schmitt, R. W. & Polzin, K. W. 1994. Estimates of diapycnal mixing in the abyssal ocean. *Science*, **264**, 1120-1123.

Trofimov, A. & Ingvaldsen, R. 2012. Hydrography. In: *Survey report from the joint Norwegian/ Russian ecosystem survey in Barents Sea August- October 2012*. Ed: Eriksem E. *IMP/PINRO Joint Report Series*, No 2/2012, Pp. 7-15.

Tsamados, M., Feltham, D. L. Schroeder, D., Flocco, D., Farrell, S. L., Kurtz, N., Laxon, S. W. & Bacon, S. 2014. Impact of Variable Atmospheric and Oceanic Form Drag on Simulations of Arctic Sea Ice. *Journal of Physical Oceanography*, **44**, 1329-1353: doi:10.1175/JPO-D-13-0215.1.

Tsubouchi, T., Bacon, S., Naveira-Garabato, A. C., Aksenov, Y., Laxon, S. W., Fahrbach, E., Beszczynska-Möller, A., Hansen, E., Lee, C. M. & Ingvaldsen, R. B. 2012. The Arctic Ocean in Summer: A quasi-synoptic inverse estimate of boundary fluxes and water mass transformation. *Journal of Geophysical Research*, **117**, C01024, doi:10.1029/2011JC007174.

Vellinga, M., Dickson, B. & Curry, R. 2008. The changing view on how freshwater impacts the Atlantic meridional overturning circulation. In: *Arctic-Subarctic Ocean Fluxes*, Eds. Dickson, R. R., Meincke, J. & Rhines, P.., Springer, Dordrecht, doi:10.1007/978-1-4020-6774-7.13.

Watson, A. J., Ledwell, J. R., Messias, M.-J., King, B. A., Mackay, N., Meredith, M. P., Mills., B. & Naveira-Garabato, A. C. 2013. Rapid cross-density ocean mixing at mid-depths in the Drake Passage measured by tracer release. *Nature*, **501**, 408-411.

Woodgate, R., A. & Aagaard, K. 2005. Revising the Bering Strait freshwater flux into the Arctic Ocean. *Geophysical Research Letters*, **32**, L02602, doi:10.1029/2004GL021747.

Woodgate, R. A., Aagaard, K. & Weingartner, T. J. 2005. Monthly temperature, salinity, and transport

Woodgate, R. A., Aagaard, K. & Weingartner, T. J. 2006. Interannual changes in the Bering Strait fluxes of volume, heat and freshwater between 1991 and 2004. *Geophysical Research Letters*, **33**, L15609, doi:10.1029/2006GL026931.

Woodgate, R. A., Aagaard, K. & Weingartner, T. J. 2007. First steps in calibrating the Bering Strait throughflow: Preliminary study of how measurements at proposed climate site (A3) compare to measurements within the two channels of the strait (A1 and A2), University of Washington, Seattle.

Woodgate, R. A., Weingatner, T. & Lindsay, R. 2010. The 2007 Bering Strait oceanic heat flux and anomalous Arctic sea-ice retreat. *Geophysical Research Letters*, **37**, L01602, doi:10.1029/2009GL041621.

Wunsch, C. & Ferrari, R. 2004. Vertical Mixing, Energy, and the General Circulation of the Oceans. *Annual Review of Fluid Mechanics*, **36**, 281-314, doi:10.1146/annurev.fluid.36.050802.122121.

Yang, K. & Comiso, J. 2007. An unexpected seasonal variability of salinity in the Beaufort Sea upper layer in 1996-1998. *Journal of Geophysical Research*, **112**, (C5): C05034, doi:10.1029/2004JC002716.

Zhang, J. & Steele, M. 2007. The effect of vertical mixing on the Atlantic water layer circulation in the Arctic Ocean. *Journal of Geophysical Research*, **112**, C04S04, doi:10.1029/2006JC003732.